UNIVERSITY OF LEICESTER

Theoretical and Experimental Study of Pure and Mixed Water Clusters using Infrared Spectroscopy

Thiviyan Thanapalasingam

Supervisor: Prof. Andrew Ellis

Research group: Spectroscopy & Dynamics

Department of Chemistry, University of Leicester, LE1 7RH

Submitted to the University of Leicester
in partial fulfilment of the requirements for the degree of
Chemistry MChem (Hons)

2016

Theoretical and Experimental Study of Pure and Mixed Water Clusters using Infrared Spectroscopy

Thiviyan Thanapalasingam

ABSTRACT

A number of previous studies have used simple molecules, such as water and methanol, as "prototypes" to understand fundamental hydrogen bonding interactions. The present investigation used resonant ion-dip infrared spectroscopy to record cluster-size-selective spectra of $(H_2O)_n$, trapped inside helium droplets. Spectra of the clusters were obtained in the range of OH stretching vibrations (3000 - 4000 cm^{-1}) as this region is sensitive to the details of the hydrogen bonding network. In order to facilitate spectral assignment, harmonic frequencies and infrared intensities were calculated for different structures of the water heptamer (n = 7) at the MP2/aug-cc-pVDZ level. The experimental IR spectrum were consistent with the harmonic approximations of the cyclic heptamer. The bonded-OH band shifts of cyclic clusters (n = 3 - 8) suggested that the cyclic-$(H_2O)_7$ is the least structurally strained ring. In addition to the spectra, the finding was supported by calculated transition dipole moments of the bonded-OH transitions and anharmonic approximations.

An *ab initio* study identified the cyclic conformation of $MeOH(H_2O)_n$ clusters, where *n* = 3-7. The methanol forms strong hydrogen bonds with water molecules owing to the electron-donating nature of the methyl group. The predicted spectra for the mixed cluster showed that the bonded-OH band is split into multiple transitions, while the free-OH band remained unaffected. The work has also discussed how these characteristic OH-stretches can be used to detect individual $MeOH(H_2O)_n$ clusters using helium droplets.

Ice is known to store hydrogen gas efficiently. This *ab initio* work carried out on the $H_2(H_2O)_6$ cluster has attempted to provide a molecular level understanding of the stabilisation that exists within hydrogen and ice. The results showed that the cyclic hexamer hydrogen framework undergoes a small structural deformation to accommodate a dihydrogen molecule. The harmonic spectrum suggested that this relieve on the H-bonds as evidenced by redshift of bonded-OH band of the cyclic hexamer.

ACKNOWLEDGEMENT

First and foremost I would like to thank my project supervisor, Professor Andrew Ellis, for making me part of a great research experience. His invaluable advice and guidance over the course of the year is greatly appreciated. His constructive feedback regarding the drafts of this work served well to better this report.

I am very thankful to Media Kakaee and Ahmed Sadoon for their help with my project. They have kindly shared their knowledge and expertise that they have gained throughout their PhD programme. My colleagues from the Spectroscopy and Dynamics group were a great source of support and motivation.

Dr Corey Evans' advice regarding the use of GAUSSVIEW and MATLAB for data analysis is appreciated. I would also like to thank Professor Joel Bowman and his group at Emory University (Atlanta, USA) for making this international collaboration possible.

Finally, I thank my parents, siblings and brother-in-law for providing me with their support and encouragement throughout my master's degree. I dedicate this work to my lovely and dear nephew, Arjun, whose laughter kept me company while working on this project.

TABLE OF CONTENTS

CHAPTER 1 INTRODUCTION

1.1. Water Clusters, $(H_2O)_n$

1.1.1. Background

Water is the foundation of all biological system. It is one of the most abundant compounds on earth, covering almost two thirds of the planet's surface and accounting for about 70% of the human body mass. Without water life would cease to exist. As it is a readily-available and inexpensive solvent, the use of water in chemical reactions has been taken for granted by chemists for decades.

Water is known for exhibiting a number of unusual properties. Usually, upon freezing a liquid its density increases as the result of the tightly bound constituent molecules. However, in the case of water it decreases because it undergoes expansion. Even though water is not the only compound to exhibit its highest density in the liquid state it possesses other characteristics that tend to deviate from that expected of a simple liquid.[1] The rapid increase in the heat capacity of water observed during supercooling of the compound means it takes less heat to raise the temperature of cold water by 1ºC compared to raise the same amount of warm water.[2] This effect plays a big part in the ocean circulation effects that influence global climates. Under pressure cold water becomes more fluid, while other substances exhibit higher viscosity when put under the same condition. The unusual characteristics of water mentioned above are just anomalies water possesses. Despite being one of the most extensively studied compound up to date,[1,3–5] the fundamental reasons behind these phenomena remain to be unknown. Water plays a key role as a solvent in many organic synthesis and its use is being encouraged for sustainable chemistry in the future.[6] Thus, it is necessary to unravel the mysteries of water.

It is clear that the hydrogen bond network and its fluctuations and rearrangement dynamics determine the properties of the liquid.[7] Therefore, an accurate description of the water intermolecular interaction is seen as one of most important problems to tackle in physical chemistry and thus, molecular level understanding of water is required.[5] A novel approach for quantitative analysis of hydrogen bond interactions is the size-selective study of the structures of water clusters [3,4,8–10]. A *cluster* refers to a group of loosely bound atoms/molecules. The nature of the intermolecular interactions encountered between the water molecules is the same in the molecular clusters as in the bulk.[11] Therefore, spectra of water clusters can be employed to investigate the intermolecular potential energy surface (PES), giving insight into hydrogen bonding in all phases of water.[12,13]

Molecular clusters serve well as a testing "prototype" for current intermolecular potentials of hydrogen-bonded molecules.[8,14]

Infrared spectroscopic studies carried out in conjunction with *ab initio* electronic structure calculations constitute a powerful technique for probing the details of these hydrogen bonding networks in clusters.[15–17] The importance is given to OH stretching vibrations in the 3000 – 4000 cm^{-1} range, which is a region sensitive to the underlying hydrogen bond network.[9] Small water clusters have been extensively studied both theoretically and experimentally. A water dimer (n = 2) forms a linear structure, while trimer (n = 3) to pentamer (n = 5) clusters have low-lying cyclic structures.[18] However, clusters start developing three-dimensional (3-D) structures, such as cage and prism, at n = 6 rather than a simple cyclic structure.[19,20] In fact, the hexamer is the smallest cluster which has many isoenergetic structures and different levels of *ab intio* theories assign these isomers different relative stabilities.[21,22] Recently, Pérez *et al.* identified the coexistence of those multiple low-energy structures of the hexamer in a pulsed supersonic expansion experiment using rotational spectroscopy.[10]

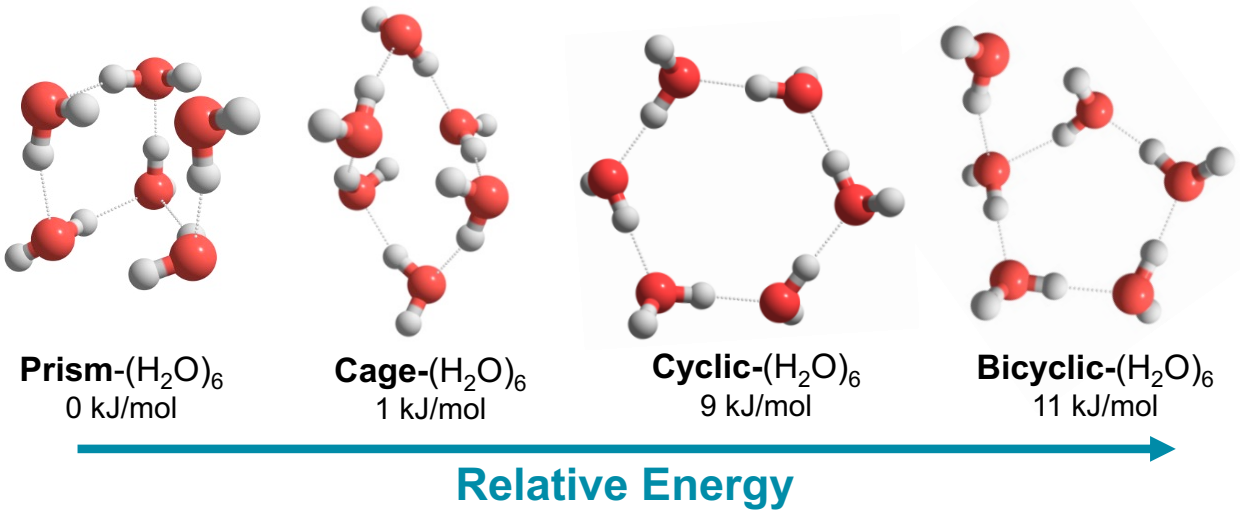

Figure 1: The commonly known conformations of the hexamer cluster (prism, cage, cyclic and bicyclic) in the order of increasing energies calculated at the MP2/aug-cc-pVDZ level.

1.1.2. Cyclic Water Hexamer, $(H_2O)_6$

Despite the structural preference for low-lying 3D isomers, in 2000 Miller and Nauta observed the cyclic form of the hexamer formed in liquid helium droplets by means of infrared spectroscopy.[15] The evidence of the hexamer arose from the additional peak red shifted relative to the pentamer band. The ring formation was hypothesised to take place via a molecular pick-up process in which sequential insertion of monomers into preformed smaller cyclic complexes takes place.[16] Miller and Nauta suggested that the water ring insertion is facilitated by tunnelling of the hydrogen atoms through associated energy barriers. Furthermore, they also proposed that the energy barrier associated with the rearrangement of the 3D hydrogen bonding network to form the cage from the subsequent ring is not overcome at the low temperatures inside liquid helium and hence the hexamer retains its cyclic structure (as illustrated in **Figure 2 b**).

In a subsequent study, their attempt to find the cyclic heptamer (n = 7) was not complete as they believed either that the red shift associated with the cyclic structures have rapidly converged and there obscured by the spectral contribution of the hexamer or that larger cyclic structures (n > 6) are simply not formed due to the lack of similar stability provided by helium.[16] Another interesting observation made in this study is the weak band at 3229 cm^{-1}, which led to Miller and Nauta believe that it may have arisen from small amount of the cage form, which managed to overcome the transformation energy barrier, or alternatively from associated with the growth of larger clusters. The theoretical work by Wang *et al.* completed the assignment of the cyclic hexamer by highlighting that the band at seen in Miller and Nauta's experimental spectrum corresponded to bend overtone, which is not predicted by double-harmonic calculation [23]. It has been 16 years since Miller and Nauta's discovery of the cyclic hexamer, but the existence of the next largest cyclic water cluster (i.e. the cyclic heptamer) remains to be a mystery.

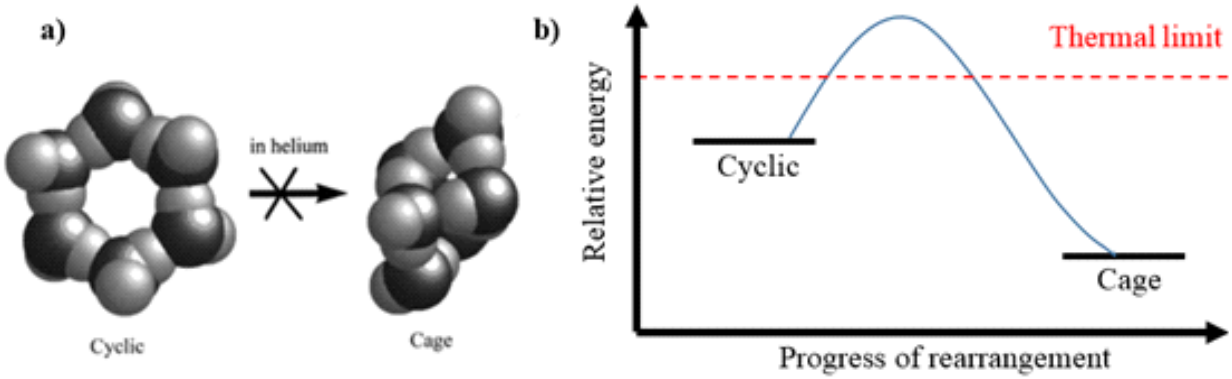

Figure 2: a) The structure of the cyclic and cage forms of the hexamer water cluster. Image was reprinted from reference [17]. b) Simplistic illustration of an energy profile diagram showing the cyclic conformer being higher in energy than the cage conformer for the hexamer.

The formation of one hydrogen bonding in a hydrogen-bonded chain *cooperatively* enhances or diminishes the strength of another hydrogen bond, which is the result of cooperative effects.[24] However, cooperative effects are not fully understood. Cyclic clusters are only related to cooperative effects of hydrogen bonding, while non-cyclic clusters are also associated with non-cooperativity effects.[25] Furthermore, the effects of cooperativity increases with the cyclic cluster size.[26] Therefore, cyclic clusters are seen as a requirement for the full understanding of cooperative effects in a network of hydrogen bonds.

1.1.3. Water Heptamer, $(H_2O)_7$

In spite the substantial collection of work on various water clusters, only a limited number studies have explored the water heptamer (n = 7) to date.[9,27–29] Theoretical studies revealed that a prism as the global minimum structure for the heptamer.[9,27] Shields *et al.* have identified prism and cage motifs for gas phase water heptamer using Broadband Fourier transform rotational spectroscopy.[28]. Optimised structures revealed the presence of four types of water monomers in the two heptamer structure: single donor-single acceptor (DA), single donor-double acceptor (DAA), double donor-single acceptor (DDA) and double donor-single accepter (DDAA).[30] These classes refer to the number of hydrogen bond accepted and donated by a water molecule in within a cluster. The oxygen atoms (O-atoms) from DDA-type monomer form relatively weaker hydrogen bonds (O-bonds) compared to the O-atoms from DAA-type, possibly due to lower available of electron density in the former.[9,21] The strength of the H-bonds was reflected in the IR spectrum via OH vibrational frequency redshifts. It was clear that the presence of different monomer types gave rise to different spectral features at different positions, producing unique fingerprint region in the IR spectrum. A theoretical study conducted by Kim *et al.* reported that the ring conformer is preferred over the low-energy conformers (cage and prism) for the heptamer only at temperatures over 150 K.[30]

1.1.4. Larger Water Clusters (n > 10)

Investigation of larger clusters is also of interest as it would help to portrait water. However, as the size of the clusters (n) increase the complexity of the multidimensional PES topology increases significantly, because the number of possible hydrogen-bonded conformations increases exponentially.[28] Thus, difficulties involved with modelling larger clusters and locating local minima on complex PES limits high quality quantum mechanical calculations to relatively smaller clusters. A systematic approach for larger clusters is required to identify most, if not all, of the possible topologies while a manual approach can be taken for relatively small cluster (n < 7). Nevertheless, Molecular Mechanical calculations made it possible to theoretically study relatively larger molecular

water clusters (n = 40 - 100).[31] It is hoped that the improved understanding of small clusters will provide a better understanding required to model larger water clusters.

1.1.5. Objective

The objective of the first part of the investigation is to study the heptamer water cluster, $(H_2O)_7$, and determine whether their existence as the cyclic conformer is possible. This will be achieved through a series of *ab intio* simulations and experimental methods involving IR spectroscopy of size-selected helium (He) beams. The structural assignment of the heptamer will be facilitated by comparing and contrasting the predicted harmonic frequencies and vibrational intensity against recorded vibrational spectrum.

1.2. Methanol-Water Clusters, $MeOH(H_2O)_n$

1.2.1. Background

Methanol is analogues to water molecules as substitution of the methyl group (CH_3) in the molecular formula CH_3OH with a hydrogen atom gives water. Methanol is also the simplest organic molecule, which can form hydrogen bonds (H-bonds) with itself and other molecules.[26] In aqueous solutions, hydrophobic molecules generally tend to aggregate to minimise their surface contact and associated surface energies with water. In methanol-water mixture amphiphilic water molecule self-organise into structures where the hydrophobic region of molecules tend to be pushed together and away from the water, enabling the hydrophilic hydroxyl group to hydrogen bond more easily to the surrounding water molecules. This leads to a number of supramolecular assemblies including micelles and columnar phases. An emerging route toward the probing of detailed molecular models of the hydrophobic interaction, hydration, and the physics of aqueous macromolecules involves the use of small clusters consisting lower alcohols as prototypes.[32]

1.2.2. Pure Methanol Cluster

Density function theory (DFT) study performed by Hagemeister *et al.* predicted the lowest energy configurations to be linear for the dimer and cyclic for the trimer through pentamer for pure methanol clusters.[14] These are similar to the structural conformations preferred by water clusters.[18] IR spectroscopy studies of methanol clusters consisting of up to six methanol molecules showed they have a cyclic conformation.[33,34] These cyclic conformation was made possible by methanol acting as a single proton donor and single hydrogen bond acceptor. Cooperative effects has also found to play a large role in stabilising these cyclic methanol clusters.[14]

1.2.3. Methanol-Water mixed Clusters

Methanol is miscible with water at all proportions by forming multiple H-bonds.[35] A number of experimental and theoretical work have clusters have been studied methanol-water clusters.[26,32,35–37] The behaviour of methanol-water system is dependent on the molar fraction of methanol (*X*) present in the bulk as result of changes in the hydrogen bonding network and in water-rich regions (i.e. low *X*) the hydrogen bond network of water is enhanced, leading to hydrophobic hydration.[38]

In 1992 Shi *et al.* have confirmed the formation of methanol-water mixed clusters inside pulsed helium droplets using time-of-flight mass spectrometry.[36] In their study, Shi and co-workers assumed that the clusters adopt cage-like conformation due to the maximum number of hydrogen bonds and its closed network structure. Huisken *et al.* found that methanol in water clusters (n = 3 - 4) act as single hydrogen bond donor and acceptor, which led them to believe that those cluster have a cyclic conformation.[37] Recently, Mandel and co-worker's theoretical study found that the binding energies of cyclic methanol and methanol-water mixed clusters are greater than that of pure water clusters owing to the electron-donating nature of the methyl group in methanol.[26]

While a lot of attention has been given to water clusters over the years, only small number of studies in the literature have reported experimental IR spectroscopy of mixed water clusters with cyclic conformations. It is believed that cyclic clusters can provide a better understanding of hydrogen bond rearrangements in methanol-water mixture and provide insights into solvation properties of larger aliphatic alcohols.

1.2.4. Objective

A theoretical study will be conducted to identify a range of cyclic water clusters containing a single methanol molecule, $MeOH(H_2O)_n$, on their Potential Energy Surface. The vibrational spectra of optimised structures will be generated and important spectral features is to be outlined. The discussion will also look at how these clusters can be formed inside helium droplets and detected.

1.3. Hydrogen-Water Cluster, $H_2(H_2O)_n$

1.3.1. Background

Hydrogen is a good energy carrier which is able to produce energy via air combustion with pure water as the only-side product. Therefore, hydrogen has been recognised as a promising source of energy for the next generation electric vehicles.[39] However, currently difficulties are encountered with the transportation and storage of hydrogen gas.[40] Thus, it is important to address these challenges in order for hydrogen economy to be a viable energy source in the future.

The commonly physical storage of hydrogen involved the compression of the gas into liquid, which requires a large amount of energy and pose potential safety risks. This led to search for alternative storage mechanisms such as chemical storage in metal hydrides and storage involving carbon nanostructure.[39] Hydrogen storage in metal-organic framework (MOF) proved to be efficient due to the porous structure that can compact the gas.[41] Since chemical storage involve the breaking and formation of H-H bonds, these processes have rates that are far too slow for modern applications.[42]

1.3.2. Storage of Hydrogen in Ice

Water naturally forms a wealth of crystalline phases at ambient and moderate pressures, these include hexagonal ice, cubic ice, stacking disordered ice with cubic and various clathrate hydrate structures.[43] Clathrate hydrates are inclusion compounds in which guest molecules are either in a cage of host molecules.[44] It was believed that hydrogen molecules were too small to support a clathrate structure until 2002 when hydrogen clathrate hydrates were discovered where hydrogen acts as the guest molecule.[45] This discovery has led to the suggestions for its use for hydrogen storage due to its maximum hydrogen storage capacity of 3.9 wt %.[45]

Ice would seem to be an ideal storage medium as it is an inexpensive and widely-available material which can be renewably sourced. Furthermore, it is also an inert material and hence would serve well for containing a flammable hydrogen gas. Among the ice structures formed in nature, the hexagonal ice is the best suited for the storage of hydrogen, because it has the lowest density (0.92 g/ML) and largest pore size (~0.23 nm in diameter).[42]

Recently, Pascal *et al.* employed Monte Carlo and Molecular Dynamic simulations to illustrate that *hexagonal ice* structures store hydrogen efficiently, achieving 3.8 wt % at 270 K.[42] The study reported that the interaction between hydrogen and water was facilitated via Van der Waals' forces, a combination of repulsion and attraction. Nguyen and co-worker's study reported that at least 99% of hexagonal ice is present in ice crystals equilibrated at T = 250 and 270 K under 1 atm pressure.[43] This means that hydrogen can be stored in ice under relatively mild conditions which renders this storage mechanism greatly economically viable.

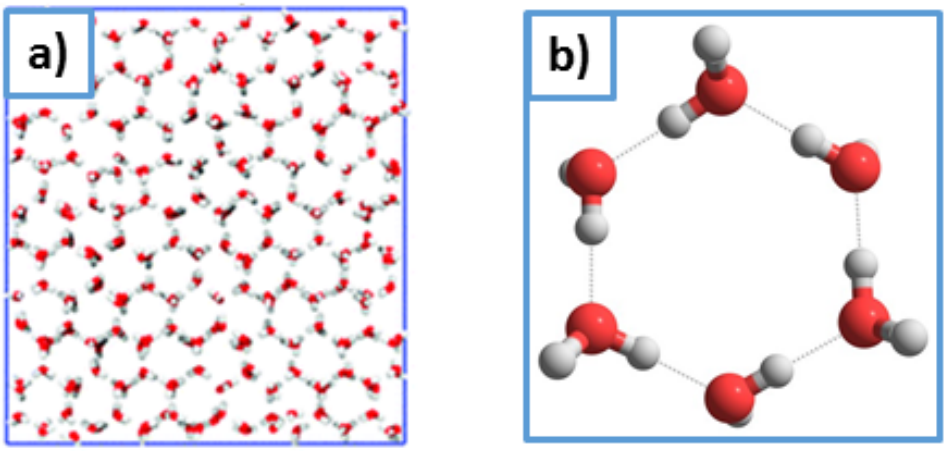

Figure 3: a) Illustration of simulated (bulk) layer of hexagonal ice. Image was reprinted from reference [38]. b) A single cyclic hexamer cluster.

However, a molecular-level understanding of hydrogen-ice interaction is still lacking. To date, studies in the literature have not employed high level quantum mechanical *ab intio* calculations to investigate this phenomenon. It is believed that the intermolecular interaction could be studied through experiments involving hydrogen-water clusters via spectroscopic studies.[4] As illustrated in **Figure 3**, the cyclic hexamer is the unit cell of the lattice structure that makes up the hexagonal ice. Thus, by focusing on clusters consisting of the hexamer ring and dihydrogen molecule insights into the efficient storage can be gained.

1.3.3. Objective

The aim of the final part of the study is to explore the molecular interaction between water cluster, specifically the cyclic hexamer, and a hydrogen molecule using *ab initio* calculations. This is to be carried out by analysing relevant structural parameters and IR spectrum of the optimised cluster.

CHAPTER 2 EXPERIMENTAL

2.1. Helium Nanodroplets (HeNds)

Helium nanodroplets (HeNds) are large molecular clusters of a few thousand helium atoms (typically 10^3 - 10^4). ^{4}He is the most abundant isotope of helium. As shown in **Figure 4**, the phase diagram of ^{4}He lacks a triple point which is usually present in other elements. Therefore, at low temperatures (< 20 K) and low stagnation pressures (< 30 bar) He undergoes phase transition from a normal liquid (He I) to a superfluid (He II).[46–48] At temperatures below 2.18K bulk ^{4}He forms superfluid. Superfluid ^{4}He possesses a number of interesting characteristics which make it as a suitable *cryogenic matrix* for high-resolution spectroscopy.[49]

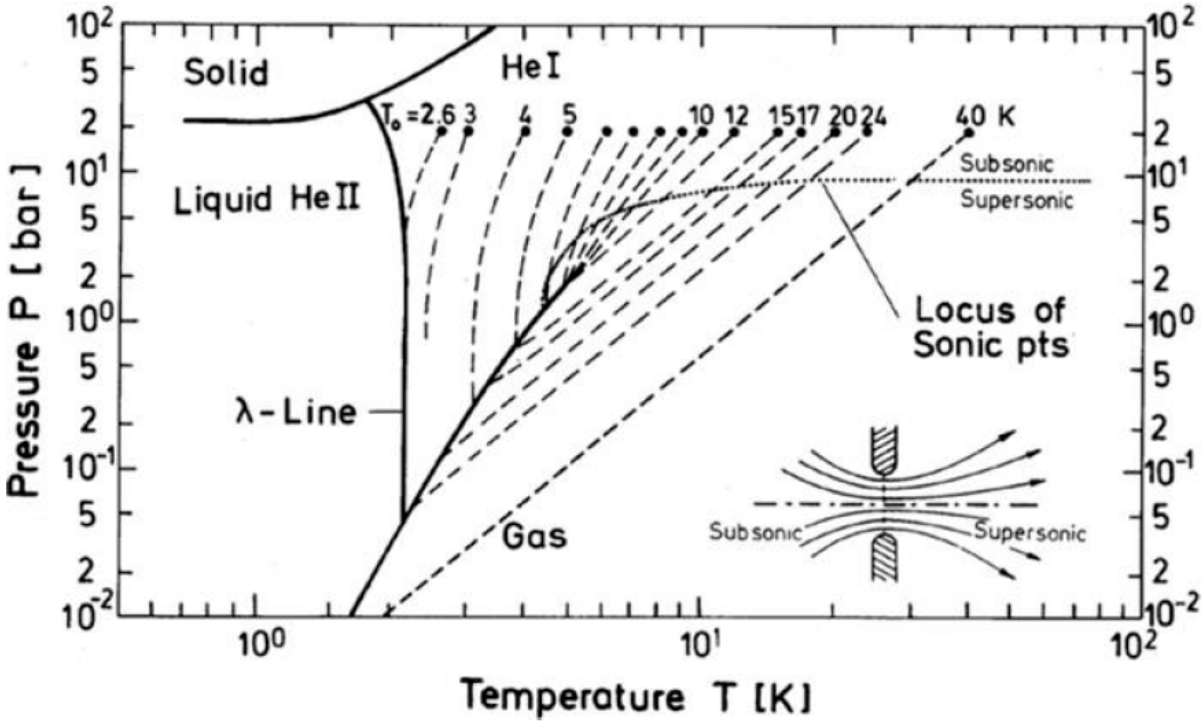

Figure 4: Phase diagram of ^{4}He representing the different phases. Dash lines represent the path that ^{4}He takes in the HeNds formation at 20 bar stagnation pressure. Image was reprinted from reference [30].

Liquid helium suffers from poor solvation characteristics making it difficult to inject molecules/atoms inside them. Unlike liquid helium, HeNds are wall-free cryostats which allows for the simple insertion (doping) of molecules into the droplet and coagulate in the interior of the droplet.[50] Molecules embedded (dopants) within HeNds may rotate unhindered inside HeNds and this mobility remains unaffected even at temperatures close to absolute zero.[51] Viscosity approaching zero means that ^{4}He provides essentially a gas-like environment for molecules. HeNds has an extremely low equilibrium temperature of 0.37 K which means that the dopants being picked

up are rapidly cooled to very low temperature. This relaxes the energy states of the captured molecules and atoms constraining them to low quantum states. As a result any hot bands that may complicate the spectral assignment can be removed.

On the other hand, ^{3}He is not a suitable cryogenic host because the droplets that this isotope forms are not superfluid. ^{3}He has a lower natural abundancy compared to ^{4}He which renders ^{3}He much more expensive than ^{4}He.

2.2. Experimental Techniques for Water Heptamer Cluster

2.2.1. Overview of the System

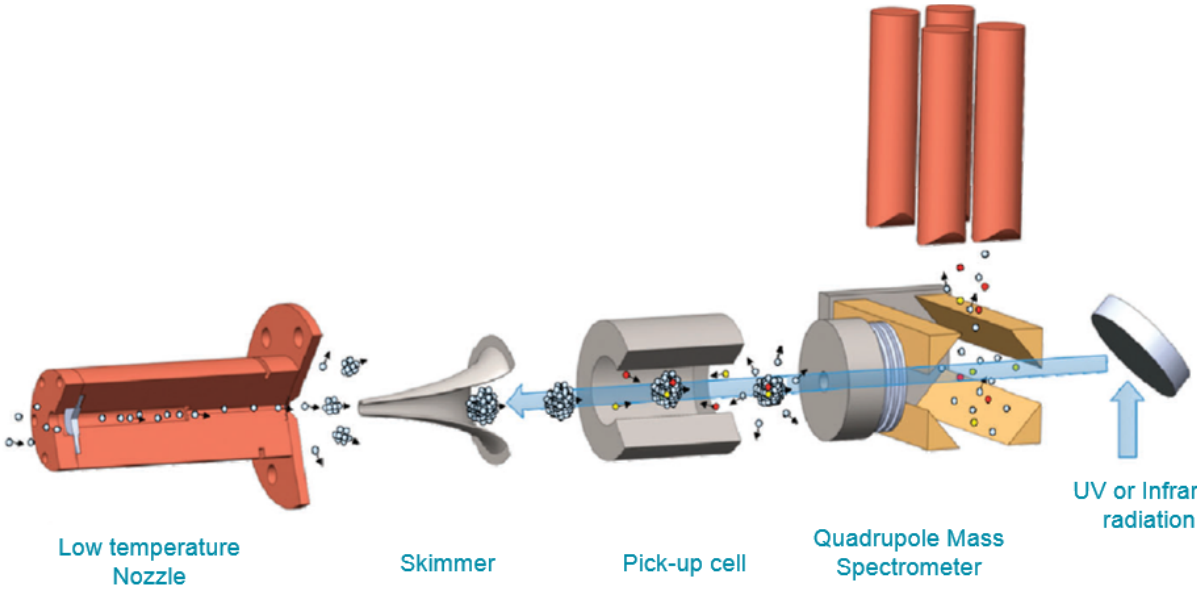

Figure 5: Simplified scheme showing the path of the He beam through the ultra-high vacuum system. Image was reprinted from reference [39].

High purity (99.9999%) He gas was precooled using a cryostat. He gas was then expanded into a vacuum at a stagnation pressure of 33 bar and nozzle temperature of 15 K through a 5 µm diameter orifice. The stagnation condition produced helium droplets with an approximate mean size of 5000 helium atoms. The He droplets were collimated into a beam by travelling through a 0.5 mm diameter skimmer before it entered the pickup chamber. As the droplets passed through the pickup cell collisions with the water vapour resulted in the pickup of water molecules. The laser was concentrated into the pickup cell using a focusing lens, so that the laser excitation of He beam occurred within the cell. Then He droplets were passed through a second skimmer (2 mm aperture) before entering the detection chamber, equipped with a Quadrupole mass spectrometer. The He beam was then ionised using electron impact (EI) ionisation and the subsequently formed ions were separated using a quadrupole mass analyser according their mass-to-charge ratio. At the end of the quadrupole the filtered ions were detected and their abundancy was recorded. IR absorption spectrum of the dopant

was recorded indirectly via dips in the ion signal measured by the mass spectrometer (*i.e.* depletion spectroscopy).

The system was equipped with several turbomolecular pumps which allowed the system reached to ultra-high vacuum (UHV) condition. The UHV system was consisted of three main vacuum chambers: (1) *source chamber* contained nozzle and first skimmer, (2) *middle chamber* contained the pickup cell and second skimmer (3) *detection chamber* accommodates the mass spectrometer. The source and the middle chambers can be vacuumed down to 10^{-5} mbar, while the detection chamber can reach as low as 10^{-8} mbar.

2.2.2. Formation of HeNds

The formation of HeNds is illustrated in **Figure 6**. The process begins with expanding pre-cooled (20-5 K) and pressurised (20 – 100 bar) He gas through a tiny nozzle into a vacuum. The ejection of the gas from a region of high back pressure to a region of high vacuum through a tiny pinhole results in expansion. This phenomena makes it favourable for the He atoms to condense into a high density molecular cluster. At this stage the droplets the undergo evaporation that the droplets cool down. *Evaporative cooling* proceeds until the energy content of the droplets is insufficient to evaporate further, losing He atoms in the process. Equilibrium temperatures close to 0.37 K are reached and thus the newly formed droplets automatically cool to a temperature which puts superfluid phase.[50] The size distribution of the HeNds is highly dependent on the cryogenic source temperature, but He concentration and source pressure also have an impact on the size.[52]

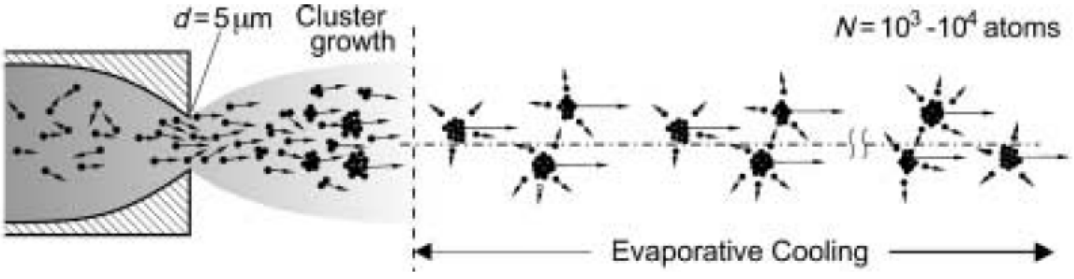

Figure 6: An overview of the formation of helium nanodroplets. *N* represents the average number of He atoms that make up the HeNds. Image was reprinted from reference [29].

2.2.3. Pickup of Water

The pickup process refers to the addition of dopant, either molecules or atoms that are of interest, to the HeNds. This occurs via simple collision with the dopants and as mentioned above, the wall-free nature of HeNds makes the pick-up possible with ease. The pickup process is a statistical process, and therefore it is not possible to obtain an exact quantity of dopant molecules or atoms

added. However, the pick-up probability follows the Poisson distribution, as shown in **Equation (1)** and therefore can be estimated.[50]

$$P_k = \frac{(\rho\sigma l)^k}{k!} exp^{(-\rho\sigma l)} \qquad \textbf{Equation (1)}$$

, where ρ is number of density of pickup gas/vapour, σ is the cross-sectional area of the HeNds (which is given by $15.5\langle N\rangle^{2/3}$ Å^2 for ^{4}He assuming a uniform density close to bulk liquid helium) and l is the length of the pickup zone. From **Equation (1)** it can be clearly seen that by scaling the experimental parameters (i.e. the pickup cell length, the pickup pressure and the size of HeNds) the probability of dopant pickup can be enhanced or reduced and thus cluster sizes can be controlled.

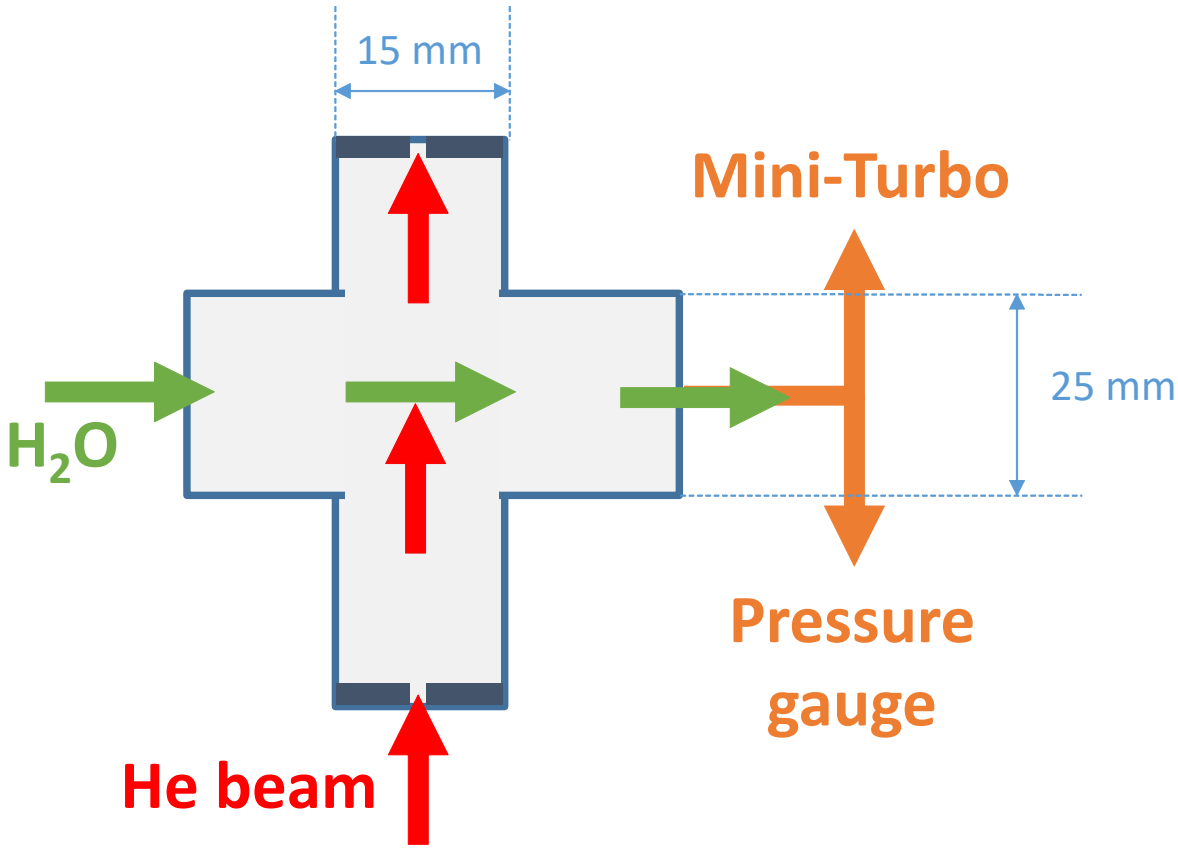

Figure 7: Simplified illustration of the water pick-up region with cell dimensions. As the HeNds travel through the pickup region (as indicated by the red arrows) they take on water molecules from the environment up on collision.

A stainless steel pickup cell was used for to add gaseous water molecules to HeNds. The cell consisted of two tubes, intersecting each other at right angle. As shown in **Figure 7**, the He beam travelled through one tube, while water was introduced externally into one end of the second tube through Swagelok connections. The other end of the second tube was equipped with a mini-turbo (TURBOVAC TMP 50; 2400 L/s) and pressure gauge (IONIVAC ITR 90). The mini-turbo ensured the pickup cell reached the optimum pressure for doping, while the pressure gauge allowed to monitor this process via changes in the pressure. The length of the pickup region that He beam passed through

was ca. 11 cm. Both ends of the cell were closed using a blank with a hole of a few mm in diameter at its centre, which allowed the He beam through the cell. At the same provided a pseudo-closed environment for the doping process, and hence minimise the amount dopant escaping into the vacuum system and allow accurate reading of the pickup cell pressure.

Gaseous water molecules were picked up by the HeNd beam when they encounter each other. As the molecules were picked they form clusters by forming hydrogen bonds. The system conditions (e.g. the pickup cell pressures and the XY alignment of the He beam source relative to the laser beam) were optimised † prior to taking IR absorption measurements, to maximise heptamer cluster formation. At 4.68×10^{-6} mBar pickup cell pressure maximum signal for the heptamer were recorded.

2.3. Mass Spectrometry of Water-doped HeNds

The formation of water clusters inside HeNds was confirmed using electron impact ionisation mass spectrometry. The electron impact kinetic energy was 70 eV. As the dopant is constantly surrounded by a shell of He atoms, direct ionisation of the dopant is very unlikely. Instead a He atom on the surface of the droplet is hit upon electron impact ionisation, leading to formation of a He^+ ion. The charge is transferred through He atoms from the surface to either of the two possible destination. (1) When the charge is transferred to the water cluster (dopant) which is usually found in the centre of the droplet or occasionally near the surface. **Equation (2)** summarises this fragmentation process of water cluster which leads to formation of protonated water clusters $(H_2O)_mH^+$, where $m = n - 1$. (2) Other, the charge can transfer to the droplet centre, where the charge attracts another He atom resulting in He_2^+ formation.[50,53] This resonant charge transfer process is called 'charge hopping'. The formation of both, the He_2^+ and protonated water cluster, release large amount of energy into the droplet. This outburst of energy results in the massive fragmentation, which terminates the charge hop process and sets the dopant free.

$$(H_2O)_n + He^+ \rightarrow (H_2O)_mH^+ + (n-m)H_2O + He \qquad \textbf{Equation (2)}$$

A Quadrupole mass-analyser (Extrel MAX-4000) was employed for the separation of ions according to their mass-to-charge (m/z) ratios. After ionisation the dopant ions were directed into a quadrupole region, where they flew up through a direct-current ramp voltage and radio-frequency (RF) voltage varying with time. The ion separation is achieved by varying the RF voltage which allowing only certain ions of specific m/z value to be detected at a time.[54] The quadrupole filter was

† The ion signal of a specific m/z was monitored in real-time using single ion mass scan (SIM) function, which allows the detection of a single mass channel.

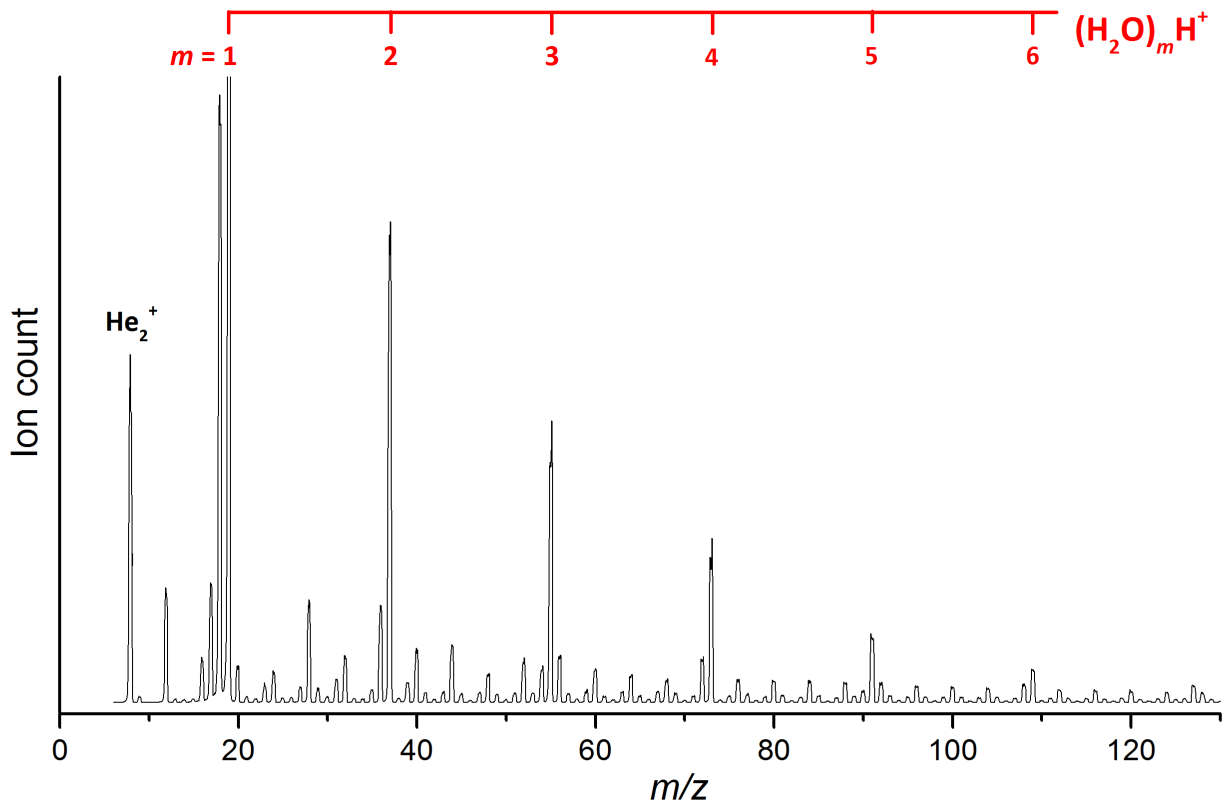

Figure 8: E.I. ionisation mass spectrum obtained of helium droplets doped with H_2O molecules. The presence of different water cluster sizes has been annotated at the top. ***m*** represents the number of water molecules in the protonated water cluster after the E.I. ionisation.

capable of detecting mass values up to 4000 Daltons. The m/z ratios and ion count were obtained using Merlin Automation™ Data System software.

2.4. Spectroscopic detection of molecules in HeNds

A pulsed Nd:YAG‡ laser (Continuum SL II-20) pumped Optical Parametric Oscillators (OPO) was used to excite molecules embedded within HeNds and depletion technique was employed to detect optical spectroscopy. The average power of the laser was 9 mJ and the delay between each pulses was 4.47 µs. The superfluid helium matrix is transparent in the entire spectral range from the far infrared (IR) to the vacuum ultraviolet (UV),[55] which made it possible to record only the spectral contribution of the molecules/atoms inside HeNds. Furthermore, the vibrational contribution resulting from the interaction of the embedded molecules with He is negligibly small.[15]

Depletion technique is commonly used to record infrared absorption spectra of dopants trapped inside HeNds.[9,56,57] IR spectrum was obtained by scanning the wavelength of the OPO laser from approx. 2500 to 3333 nm, covering the 3000-4000 cm^{-1} range. When the wavelength of the laser resonates with the vibrational frequency of the cluster, energy becomes absorbed by the water doped

‡ Neodymium-doped Yttrium Aluminium Garnet (Nd:YAG)

droplet and stored within the droplet in the form of heat. The excessive heat is dissipated via evaporative cooling and subsequently helium atoms are lost from the droplet. Since the ion signal following E.I. ionisation is proportional to the size of the HeNds (*i.e.* electron-impact cross section form ionisation), the absorption signal was detected as a dip in the mass spectrometer signal.[50]. This technique is called the resonant ion–dip IR spectroscopy (RIDIRS). With the use of ion depletion the $(H_2O)_mH^+$ ions can be monitored to the corresponding IR spectrum arising from neutral clusters with $n \geq m + 1$. Subsequently, the contribution from smaller clusters are stripped out. A relatively low pickup pressure was used for the IR measurement of the heptamer minimum formation of larger clusters.

2.5. Theoretical approach

2.5.1. Background

The second-order Møller–Plesset perturbation (MP2) theory is popular for theoretical work involving water clusters because it is the cheapest *ab initio* method that is able to describe non-covalently bound systems.[27] MP2 deals with electron correlation well and also captures all the important features of water clusters. Perturbation theory approximates solutions to the Schrödinger equation by adding corrections (i.e. *perturbation*) to a problem that slightly varies from another solvable problem.[58] Although MP2 theory provides good approximations, it is computationally demanding and requires long processing times. Density functional theory (DFT), commonly the B3LYP functional, is a faster alternative to MP2 to perform calculations on water clusters.[26] However, DFT does not represent the hydrogen bonds well because electron correlation is not dealt systematically by the theory.[59]

A number of studies in the literature employed calculations at the MP2/aug-cc-pVDZ level to optimise water clusters.[15,28] Dunning's augmented correlation-consistent polarized valence orbital basis set of double zeta (aug-cc-pVDZ) captures the hydrogen bonding very well in water clusters.[60,61] The unpaired electrons on oxygen atoms in water would result electron-electron repulsion (i.e. affects electron distribution in the molecule), which is accurately described by the basis set augmented diffuse functions. The Dunning's basis set is a split valence basis set where only the valence orbitals are presented by double basis functions. This cuts the computational cost by focusing mainly on the chemically relevant valence orbitals, while giving little importance core orbitals.

All calculations in the present investigation were carried out at the MP2/aug-cc-pVDZ level, unless stated otherwise. All calculations were performed on Gaussian 03[§] and visualised using ChemCraft software. The harmonic vibrational frequencies and band intensities were calculated for all optimised clusters. The subsequent simulated IR spectra were presented in graphical plots, where the vibrational frequency lines were broadened using Lorentzian function with a line width of 5 cm^{-1}. Throughout the text, bond lengths are in Ångströms and bond angles are in Degrees.

2.5.2. Modelling Water Clusters, $(H_2O)_n$

As shown in **Figure 9**, the structures of the cyclic clusters were modelled by adding on water molecule to a smaller, pre-optimised ring structure (e.g. the cyclic hexamer was modelled by adding a water molecule to the cyclic pentamer cluster). This theoretical approach to forming the rings is similar Miller's proposed ring-insertion mechanism [16]. Following the addition of a water monomer to the pre-existing cyclic ring, minor modifications to the structure were made prior to the optimisation where necessary. The changes include opening up the ring, to increase the likelihood of

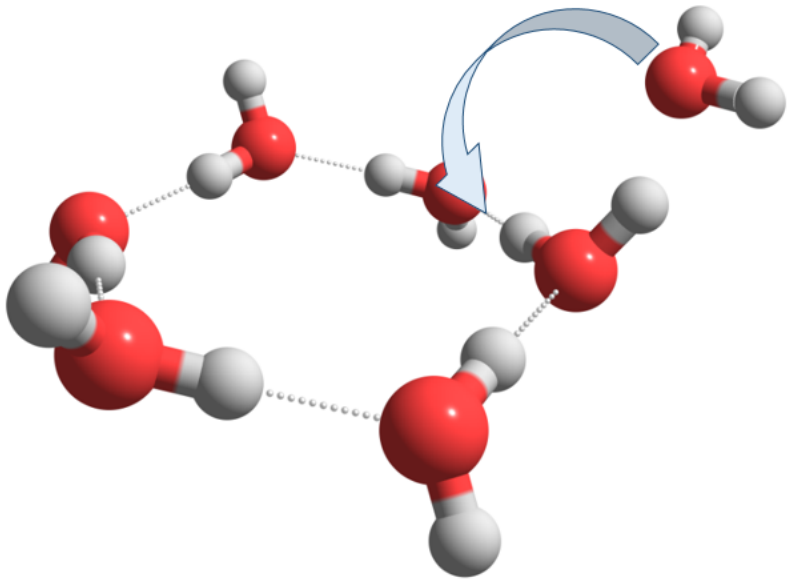

Figure 9: Simple illustration showing the formation of the cyclic hexamer via the insertion of a water monomer to yield a cyclic hexamer. Arrow illustrates the ring insertion

the water monomer being, accepted into the ring and tilting the orientation of a few water molecules, to increase the hydrogen bonding around the cyclic structure. This procedure was used to model the cyclic water clusters from trimer (n = 3) up to the octamer (n = 8).

[§] This research used the ALICE High Performance Computing Facility at the University of Leicester.

2.5.3. Modelling Methanol-Water Clusters, $MeOH(H_2O)_n$

The initial structures for the cyclic methanol-water clusters were modelled by inserting a methanol molecule near pre-optimised cyclic water clusters (from previous section). The methanol was placed so that the hydroxyl part of the molecule was pointing towards the cyclic water cluster while the methyl group was away from the ring. The water molecules in the cluster were modified as described above to encourage methanol insertion into the ring. This procedure was used model to the cyclic methanol-water clusters from trimer (n = 3) up to the octamer (n = 7).

2.5.4. Modelling Hydrogen-Water Cluster, $H_2(H_2O)_n$

The structure for the $H_2(H_2O)_6$ cluster was modelled by inserting a dihydrogen molecule in the centre of a pre-optimised cyclic hexamer as Pascal and co-worker's finding suggested that hydrogen occupies interstitial sites.[42] The optimisation were carried out using the same method/basis set described above.

CHAPTER 3 RESULTS & DISCUSSION

3.1. Water clusters, $(H_2O)_n$

3.1.1. Optimised Cyclic Cluster Geometries

Figure 10 presents the optimised cyclic clusters geometry of the water clusters, from trimer (n = 3) up to the octamer (n = 8). As with the cyclic hexamer, the hydrogen bonding interaction arise between the hydrogen atoms from one monomer and an oxygen from a different monomer. Apart from the cyclic geometry these clusters have another thing in common: Every water monomer within the ring are of the single donor-single acceptor (DA) type and O-H groups that donate a hydrogen bond (called *bonded-OH*) and those that do not (called *free-OH* and *'dangling' OH*).[62] Therefore, one can expect a relatively simpler spectral contribution from these cyclic clusters as all bonded-OH stretches will occur at similar frequencies while the free-OH stretches will form separate band; resulting in two bands within the 3000 and 4000 cm^{-1} region of the IR spectrum. These cyclic structures are quasi-planar and they possess permanent dipoles which cuts through the centre of the ring at different angles. The direction and scale of the permanent dipole varied for every cluster size due to the varying degree of symmetry of the rings.

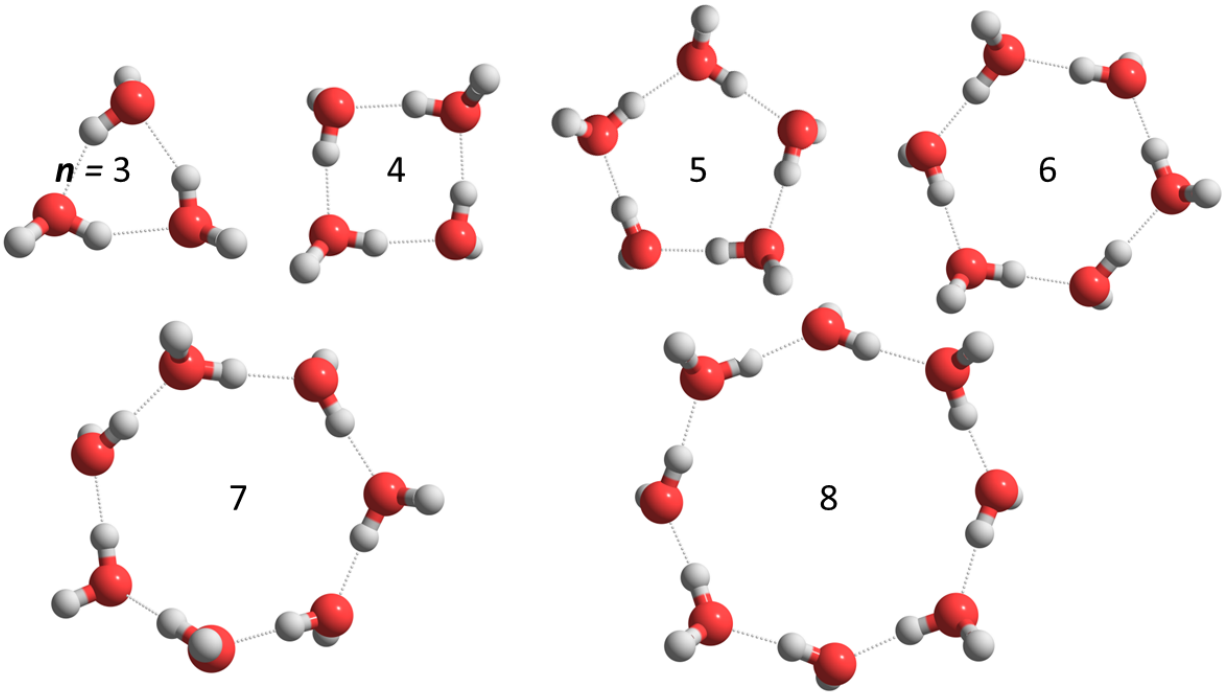

Figure 10: Top view of the optimised structures of the water clusters presented in the order of increasing cluster size; from the trimer (top-left) up to the octamer (bottom-right). ***n*** refers to the number of water monomers. The dotted lines between each monomers in a ring represent the hydrogen bonds.

3.1.2. IR Spectroscopy of Water Heptamer Cluster, $(H_2O)_7$

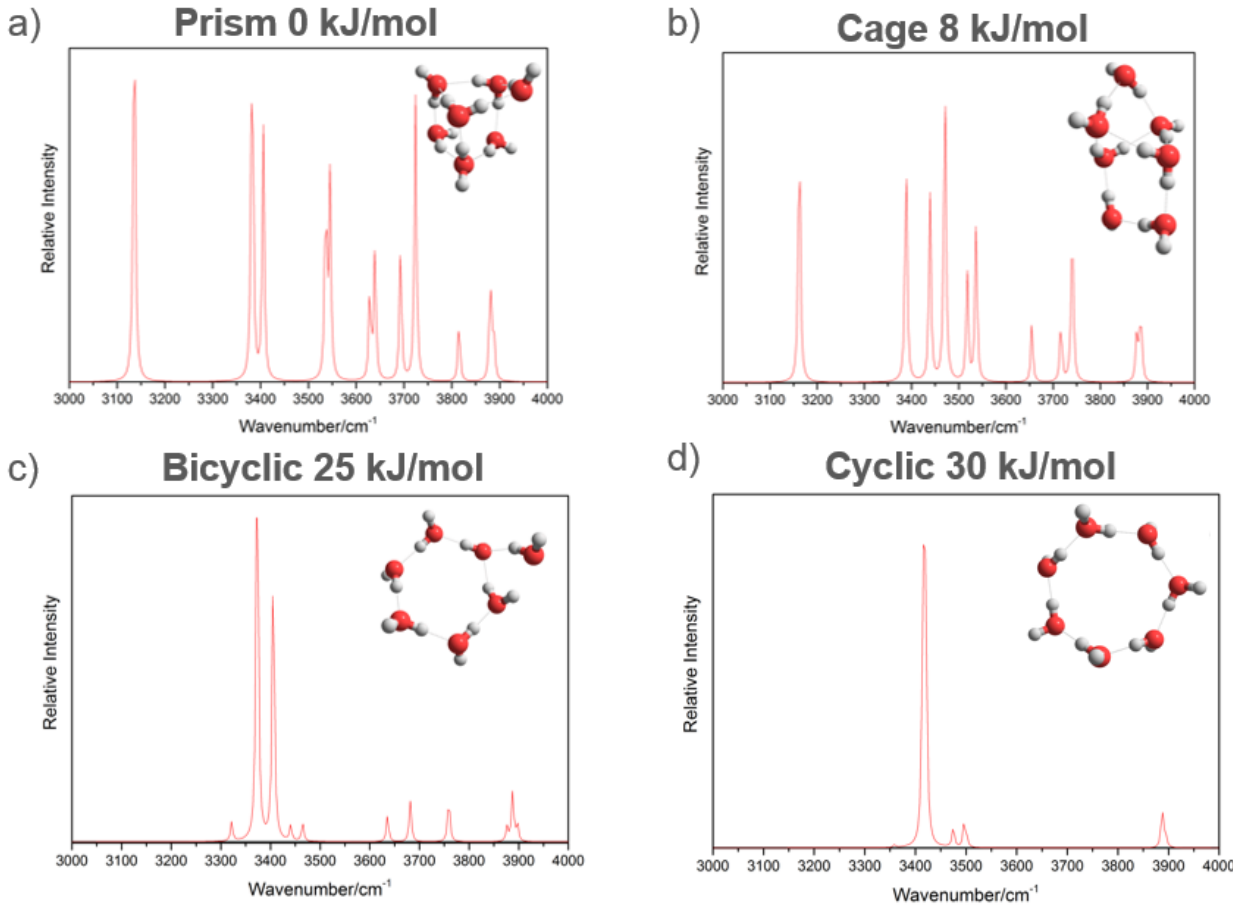

Figure 11: Optimise geometry of the different structural isomers of the heptamer cluster and their corresponding spectra and relative energies calculated at MP2/aug-cc-pVDZ.

Figure 11 presents different structural conformers of the heptamer and their corresponding spectra. The energies of the conformers increases in the following: prism < cage < bicycle < cycle. The 3D forms (prism and cage clusters) are mainly consisted of three-coordinated water monomers, a combination of DAA and DDA types. These structures lack symmetry and therefore, have a large number of different O-H 'environments' present within the cluster. These will leads to the OH stretches vibrating at different wavenumbers, giving rise to the complicated spectral features as seen in **Figure 11 (a)** and **(b)**. Although the bicyclic cluster, a structure almost identical to the cyclic conformer, was mainly dominated by two-coordinated molecule (DA), the presence of one DDA molecule gave rise to extra bands. The cyclic heptamer, on the other hand, only consisted of DA type monomers which rendered it virtually symmetrical as seen in **Figure 11 (d)**. The high symmetry of cluster meant that there only two prominent bands in the simulated IR spectrum, those corresponding to the free-OH and bonded-OH stretches.

The simulated spectra were compared with the experimentally recorded IR spectrum of the heptamer cluster. The experimental IR absorption data did not show very complex absorption patterns, which meant that the observed bands could not have stemmed from the vibrations of the prism and cage conformers. In the simulated spectrum of the bicyclic heptamer the 3300 – 3500 cm^{-1} region contained two strong transitions separated by ca. 50 cm^{-1}, which were not consistent the experimental observation. Consequently, the structure was narrowed down to the cyclic conformer.

Since the vibrational data predictions was based on the simple harmonic oscillating (SHO) model, appropriate scaling factor were required to account for the discrepancy between theoretical and experimental OH frequency shifts. To obtain suitable a scaling coefficient, the predicted vibrational frequencies for the cyclic hexamer cluster obtained from *ab intio* calculations were compared to the experimentally determined IR data recorded by Miller *et al*.[16] A comparison of the different scaling factors that were tested is shown in **Table 1**. Unfortunately, it was not possible to fit the theoretical data to the obtained IR values using a global scaling factor. The theory was in good agreement with the experimental data when the theory was adjusted using two separate scaling factors: 0.972 for free-OH stretches and 0.955 for the bonded-OH stretches.

Table 1: Impact of employing different scaling factors on vibrational data and the experimental data obtained by Miller *et al.* for the cyclic hexamer from reference [16].

Experiment		**Theory (MP2/aug-cc-pVDZ)**		
Bonded-OH	Free-OH	Scaling Factor	Bonded-OH	Free-OH
3335	3717	0.955	3277	3716
		0.972	3335	3782
		0.972 & 0.955	3335	3716

The two scaling factors were used to adjust the predicted band wavenumbers of the cyclic heptamer. As shown in **Figure 12**, a good agreement was observed between the scaled theory and experiment for the cyclic heptamer. The strong vibrational bands observed in the experiment at approx. 3321 and 3726 cm^{-1} could correspond to the bonded-OH and free-OH stretches, respectively. The two minor peaks predicted to be between 3360 and 3330 cm^{-1} were not visible on the recorded spectrum; likely due to the noise or fluctuations in the signal. The band at ca. 3235 cm^{-1} observed in the experiment was not predicted by the theory. This band was in a similar region of the spectrum to

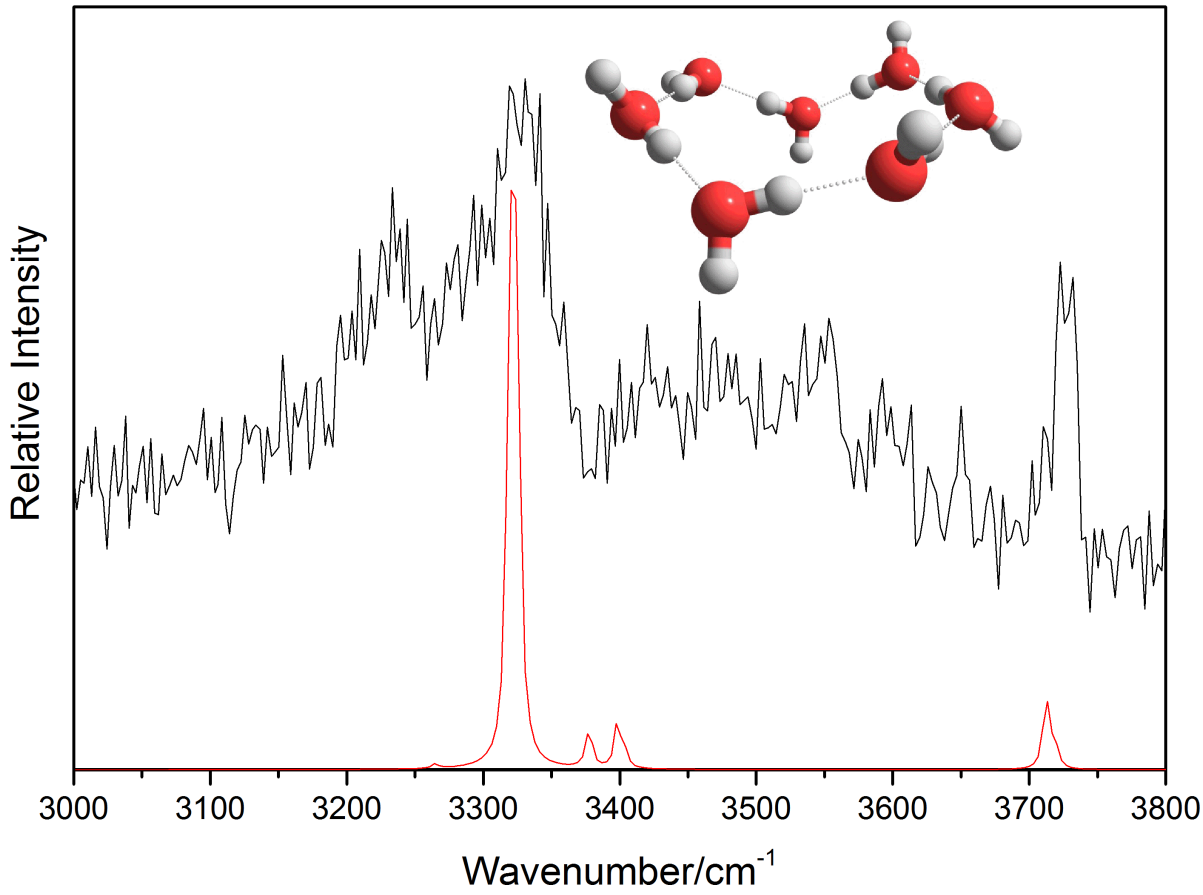

Figure 12: Graphical plot of the theoretical prediction (red line) and the experimental data (black line) recorded for the water heptamer. Two different scaling factors were used: 0.972 for the bonded OH-stretches and 0.955 for the free-OH stretches. A perspective image of the cyclic heptamer is shown on the top-right corner.

the one observed by Bowman *et al.*,[23] which was assigned to the water bend overtone transition of cyclic hexamer. It was believed that the heptamer may also produce a similar bend overtone transition which accounts for the band at 3225 cm^{-1}. This band was not predicted by the calculations which were based on the harmonic oscillator due to the anharmonic origin of the bend overtone.

The bands observed in the experiment were not of a symmetrical nature (*i.e.* did not have a Gaussian-like shape). Therefore, the experimental vibrational wavenumbers of vibrational bands were determined at the middle point of full width line at half height. There were two different sources of error in the experimental measurements. Firstly, the laser when not calibrated properly can produce readings which are offset by a few wavenumbers from the true values. The second source of error arises when reading wavenumbers from IR spectrum (i.e. human error). It is believed that human error is likely to introduce a larger error margin than the laser-offset as the noise made it difficult to obtain exact values. The present investigation employed continuous-wave He beam to yield a spectra with a reasonable the signal-noise ratio, with. The significant noise contribution can be attributed to the use of low water content employed to minimise IR interference from larger water clusters.

Slipchenko *et al.* reported that pulsed beam help produce spectrum with the signal and signal-to-noise ratio by more than a factor of 100 compared under same experimental conditions.[63] Thus, replacing the current nozzle with a pulse nozzle it may be possible to pulsed depletion spectra with reduced noise.

Despite the good agreement between the experimentally measured and predicted wavenumbers, the ratio of the predicted bonded-OH and free-OH band intensities were not in agreement with that observed in the experimental data. Theory predicted a signal intensity for the bonded-OH about 10 times that of the free-OH band. In contrary, the experiment did not show a large difference in the signal intensities. To investigate the cause of this inconsistency, the harmonic vibrational frequencies and band intensities for the cyclic heptamer were predicted using single-point geometry calculations using Hatree-Fock (HF) and Density Functional Theory (B3LYP functional) theory. The comparison of the spectra revealed that the inconsistency in the peak intensity proportionality did not arise as result of using the MP2 theory. In fact the vibrational intensities predicted by the three theories were almost identical. The vibrational frequencies predicted by MP2 and B3LYP seems to be in good agreement. However, HF approximations overestimated the vibrational frequencies by approx. 15%. This was expected from HF theory since the energy minimisation occurs by variational theorem, always leading to an energy value higher than the true energy ($E_{HF} > E_{true}$). This may need further investigation to understand the nature of the discrepancy arising in the signal intensities.

3.1.3. Transition dipole moment

Miller *et al.* have identified a peak at 3321cm^{-1} just on the red-side of the cyclic hexamer [16]. This peak was pressure dependent and became more prominent at the highest water pressure. As the intensity of the band increased upon the application of an electric field, the corresponding cluster was suggest to be a polar cluster. Stark measurements carried out by the group showed that the transition dipole moment of the corresponding cluster was *parallel* to the permanent dipole moment. Initially the Miller and co-workers thought that they captured cage conformer of the hexamer, but their *ab initio* work showed that the book conformer had a *perpendicular* transition dipole moment. Therefore, a definitive assignment for the band observed by Miller *et al.* was not possible given the wide range of isomers of the hexamer and others clusters that could have been formed inside helium nanodroplets.

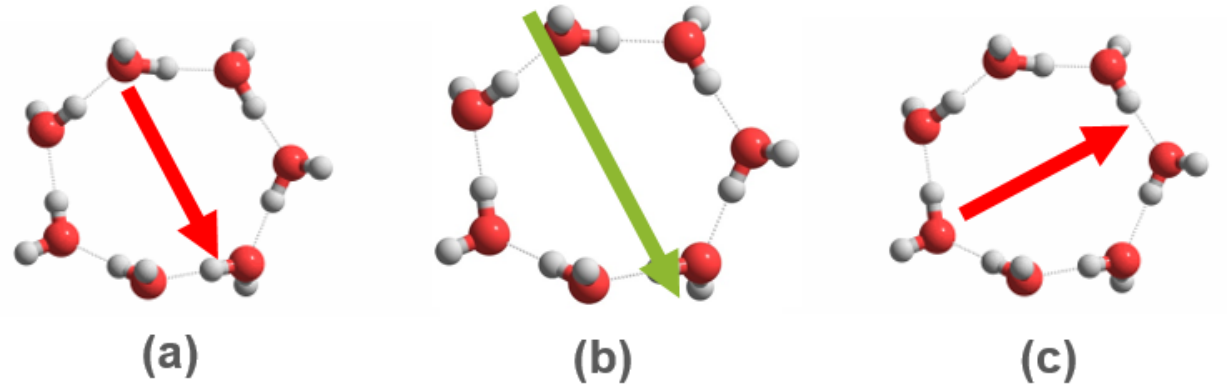

Figure 13: The directions of the transition dipole moments are illustrated by the red arrow as predicted by the MP2/aug-cc-pVDZ level calculations for both transitions, **(a)** at 3415 cm^{-1} and **(c)** 3421 cm^{-1}. The direction of permanent dipole moment in the cyclic heptamer are presented by the green arrow in **(b)**. *The scale of the arrows do not reflect on the magnitude of the dipole moments.*

In the present investigation, the experimentally determined vibrational wavenumbers of the bonded-OH of the cyclic heptamer lies at approx. 3320 cm^{-1}. As the cyclic heptamer was a quasi-planar cluster and consequently lacks some degree of symmetry, it possess a permanent dipole moment of 0.963 Debye. The theory predicted that the bonded-OH band was consisted of two vibrational transitions of equal intensity, separated by approx. 5 cm^{-1}. The direction of the transition dipole moments of two vibrations was *estimated* using dipole derivatives (i.e. the change in the dipole moment during a vibration). As shown in **Figure 13**, the results indicated that the vibration corresponding to the higher wavenumber possesses a transition dipole moment that was perpendicular to the permanent dipole moment, while the one at lower wavenumber was parallel. These results clearly indicated that the transition at higher frequency agreed with the assignment, while the alternative disagreed. As the transition dipole moment is along the permanent dipole moment it is likely that the higher wavenumber transition stemmed from the cyclic heptamer. It is believed that the stark measurements were carried out by Miller *et al.* belongs to this transition.[16]

Miller and group's investigation used an IR spectroscopic technique, which did not have any means of selectively recording the spectral contribution of the heptamer causing interference from hexamer cage.[16] However, the present study employed RIDIRS that selectively monitored depletion signal from $H^+(H_2O)_6$ ions to extract the spectrum for neutral heptamer. This allowed the contribution of smaller clusters ($n < 7$) to be stripped away from the heptamer spectrum. As larger water clusters ($n > 7$) could also fragment and produce $H^+(H_2O)_6$ ions their OH stretching vibrations interfere with the spectrum. However, those interference was assumed to be negligible since low pressure conditions (i.e. low water content) was used to encourage heptamer formation over larger clusters.

Given the evidence discussed above, it can be concluded that the cluster corresponding to the band at 3321 cm^{-1} observed by Miller *et al.* could have arisen from the presence of the cyclic heptamer in their experiment. The assignments were based on the assumption that the band observed at 3321 cm^{-1} in the present investigation is the same as the one recorded by Miller and co-worker at the same wavenumbers.[16] Nevertheless, with the use of a 'Mutlipass Stark cell' it would be possible to perform Stark spectroscopy of the heptamer cluster in a follow-up work to determine the *actual* transition dipole moment of the transition at 3321 cm^{-1} recorded in this study.[64]

3.1.4. Structural Strain within Rings

Figure 14 shows a plot of the experimentally determined and theoretically predicted bonded-OH stretching wavenumbers for different cluster sizes, from trimer (n = 3) to octamer (n = 8). The

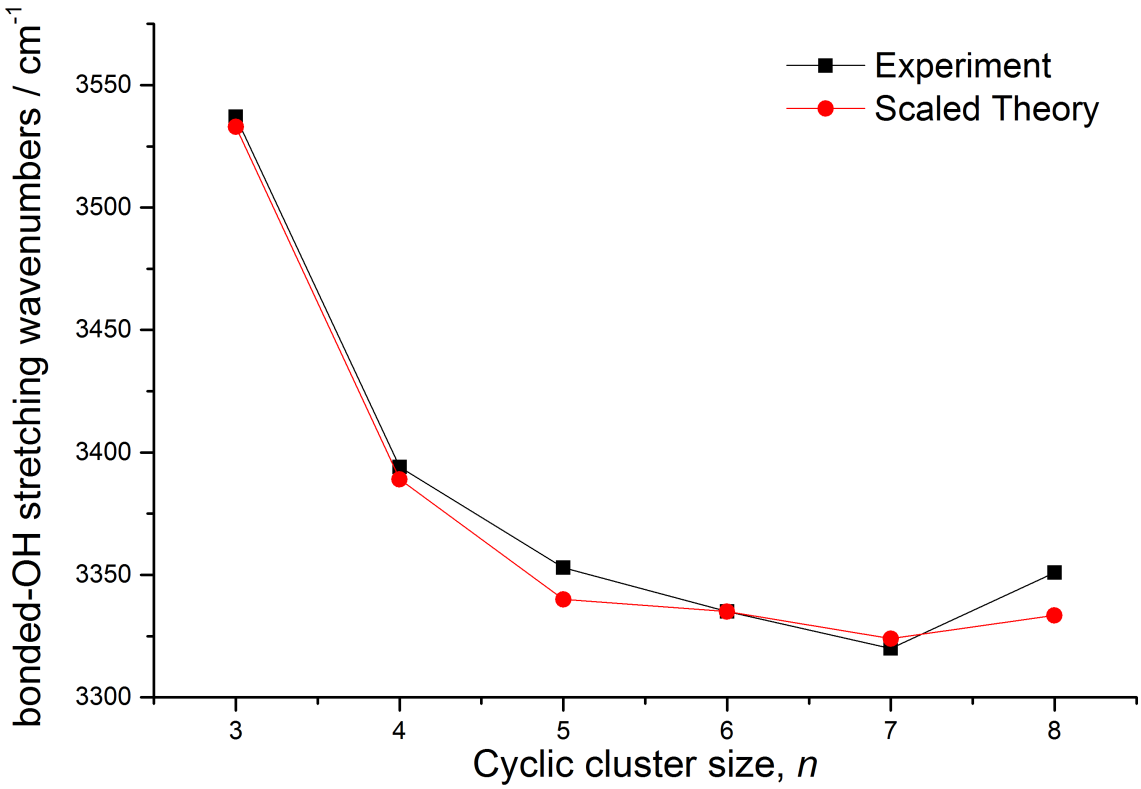

Figure 14: Relative band positions of the bonded-OH stretches, from trimer through to the octamer water clusters. A scaling factor of 0.972 was applied to account for the harmonic vibration model of the bonded OH stretches.

experimental data were in good agreement with the scaled-vibrational wavenumbers. Shifting of the bonded-OH bands is an indicator of strain on the H-bonds of cyclic clusters.[4,65] As the ring size increases from n = 3 to n = 7 bonded-OH bands shift toward lower wavenumbers (i.e. redshift) indicating a reduction in the strain on the H-bonds. This has suggested that the structural strain decreases from trimer to the heptamer rings. Similar trends were also observed in the predicted

lengths of the H-bonds. The average H-bond length reduced from trimer (~ 1.909 Å) to heptamer (~1.740 Å), indicating strengthening of H-bonds. Thus, the bonded-OH stretching frequencies are inversely proportional to the strength of the H-bonds.

The redshifts of the bonded-OH bands converges with increasing ring size. This could be an indication that the relief in the structural strain is reducing as the cyclic cluster grows. An increase in the ring size from the heptamer to octamer resulted in the reversal of the bonded-OH redshift. The blueshift of the stretches suggested that the structural strain is higher in the cyclic octamer. This means the heptamer ring experiences minimum structural strain compared to the cluster sizes and thus, the cyclic heptamer possesses minimum strain energy in addition to the normal internal energy of the cluster. The OH redshift can also be associated with the weakening of the H-bonds when new H-bond are formed (i.e. cooperativity effect).[24]

Attempts to optimise cyclic structures for the nonamer (n = 9) clusters were made by the insertion of water monomers to the optimised octamer ring. A cyclic structure was obtained for the nonamer at the HF/6-31G level, but at a MP2/aug-cc-pVDZ level of the same model the geometry optimisation returned a bicyclic structure consisting of a hexamer and pentamer rings fused together (shown in **Figure 15**). The fact that a bicyclic structure is preferred over cyclic can be attributed to the larger flexibility provided by the Dunning's basis set (aug-cc-pVDZ) on the basis functions, which helps the nonamer to minimise to a lower-energy bicyclic conformer rather than being confined to a cyclic structure. Nevertheless, the fact that the large ring cannot be obtained via geometry

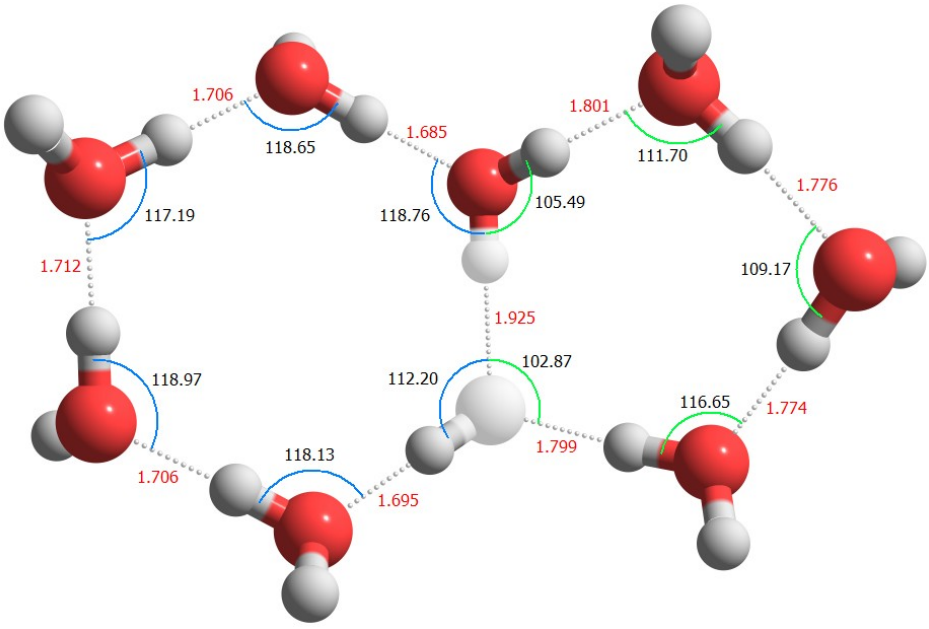

Figure 15: A top view of the bicyclic nonamer structure obtained from a MP2/aug-cc-pVDZ level optimisation with the corresponding structural parameters: lengths of hydrogen bonds (red text) and internal angles of the rings.

optimisation can be attributed to structural strain as it may be the case that the structural strain increases rapidly after n = 8. The preference for the bicyclic structure could mean that the combined structural strain in its rings is less than that of the nonamer ring. However, to investigate this hypothesis a theoretical model of the cyclic nonamer cluster is required.

It should be stressed that this is not a conclusive proof that the cyclic form of the nonamer does not exist at the MP2/aug-cc-pVDZ level. It is rather an indicator of the difficulty involved in locating a local minima with a cyclic structure due to the complex potential energy surface topology of the nonamer cluster. An efficient way to tackle this problem would be to employ Molecular Mechanics (MM) to construct *disconnectivity graphs* containing every possible structures of the water clusters in the order of decreasing energy.[66] This was successfully carried out by Miller *et al.* on tetramer, pentamer and hexamer to understand the relationship between the stationary points on the PES of water clusters.[16] MM is capable of performing geometry optimisations much faster than *ab initio* methods because the former makes use of force fields to find energy minima, ignoring Quantum Mechanics.[58] In the case of the nonamer cluster the use of MM could provide stable cyclic geometries, if any exists, that could be sampled using *ab initio* methods.

3.1.5. Anharmonic Approximation

Vibrational wavenumber calculations** based on the anharmonic rotor were obtained for cyclic clusters ($3 \leq n \leq 7$) which are presented in **Figure 16**. As these spectra are based on anharmonic approximations and portrait real vibrations more accurately than the SHO model, the frequencies were not scaled. The three bands (bend overtone stretches, bonded and free OH stretches) observed in the experiment were also encountered in the anharmonic calculations. The main advantage of anharmonic approximation over the harmonic is that the former was able to predict the band corresponding to the bend overtone.

For the different cyclic clusters the anharmonic approximation predicted free-OH band which were inconsistent with each other. This observation conflicts with the recorded experimental data and harmonic calculations, where the free-OH band remained fixed at one position (approx. 3717 cm^{-1}). Miller *et al.* have reported similar consistency in the free-OH bands between different ring sizes from their experimental and theoretical spectra.[16] The free-OH peak shift is usually independent from the cluster size, because cluster size has very little or no impact on the dangling OH bonds. Since the position of the free-OH stretches derived from anharmonic calculation varied approx. 20 cm^{-1}, it was a reasonable assumption that the uncertainty in the approximation were 20 cm^{-1}.

** Calculations were performed by Joel Bowman *et al.* at Emory University (Atlanta).

Table 2: The vibrational information predicted by experiment, the scaled-harmonic and anharmonic approximations for the cyclic heptamer, $(H_2O)_7$.

	Vibrational Bands		
	Bend Overtone	Bonded-OH	Free-OH
Scaled-Harmonic	-	3324	3713
Experiment	3225	3321	3726
Anharmonic	~3210	~3405	~3710

The vibrational data for the cyclic heptamer are presented in **Table 2**. As previously mentioned, the experimental and harmonic data were in good agreement apart from the absence of the bend overtone from the harmonic spectrum. The bend overtone band wavenumber predicted by anharmonic calculation 13 cm^{-1} redshifted to a band observed in the experiment at the 3225 cm^{-1}. Given that this value is within the 20 cm^{-1} uncertainty of the anharmonic approximation it is reasonable to suggest that recorded band corresponds to the OH bend-overtone transitions. The free-OH stretches predicted by anharmonic approximations were also in agreement with the experiment and harmonic approximation within the 20 cm^{-1} uncertainty.

However, a large discrepancy of ca. 80 cm^{-1} existed in the wavenumbers corresponding to the bonded-OH between the anharmonic approximations and experiment. In the anharmonic spectra, the bonded-OH band shifted towards the red and came to a turning point at the pentamer (n = 5) before shifting back to the blue. On the other hand, the experimental data and scaled-harmonic approximation have shown that this reversal occurs at n = 7 (as shown in **Figure 14**). The discrepancy in the OH-stretching wavenumbers can accounted for by two factors. Firstly, the anharmonic approximations were not on the cyclic heptamer geometry optimised in this investigation. Given that the bonded-OH stretches are sensitive to geometry changes it possible that the geometry differences cause the wavenumber discrepancy. Secondly, the anharmonic calculations were not performed using the MP2 theory and this may have a small impact in the discrepancy. The calculations were carried out using the *Local Monomer model*, which is based on a full-dimensional ab initio potential energy surface and dipole moment surface.[23]

It is advised to perform anharmonic vibrational frequency calculations based the optimised structures presented in this investigation. Those approximations may provide spectra that are more suitable to compare directly to the experimental and harmonic spectra. Nevertheless, the importance of anharmonic approximations lie with the power to predict the bend overtone stretching

wavenumbers. The anharmonic prediction for this band was in agreement with the experiment and harmonic approximations.

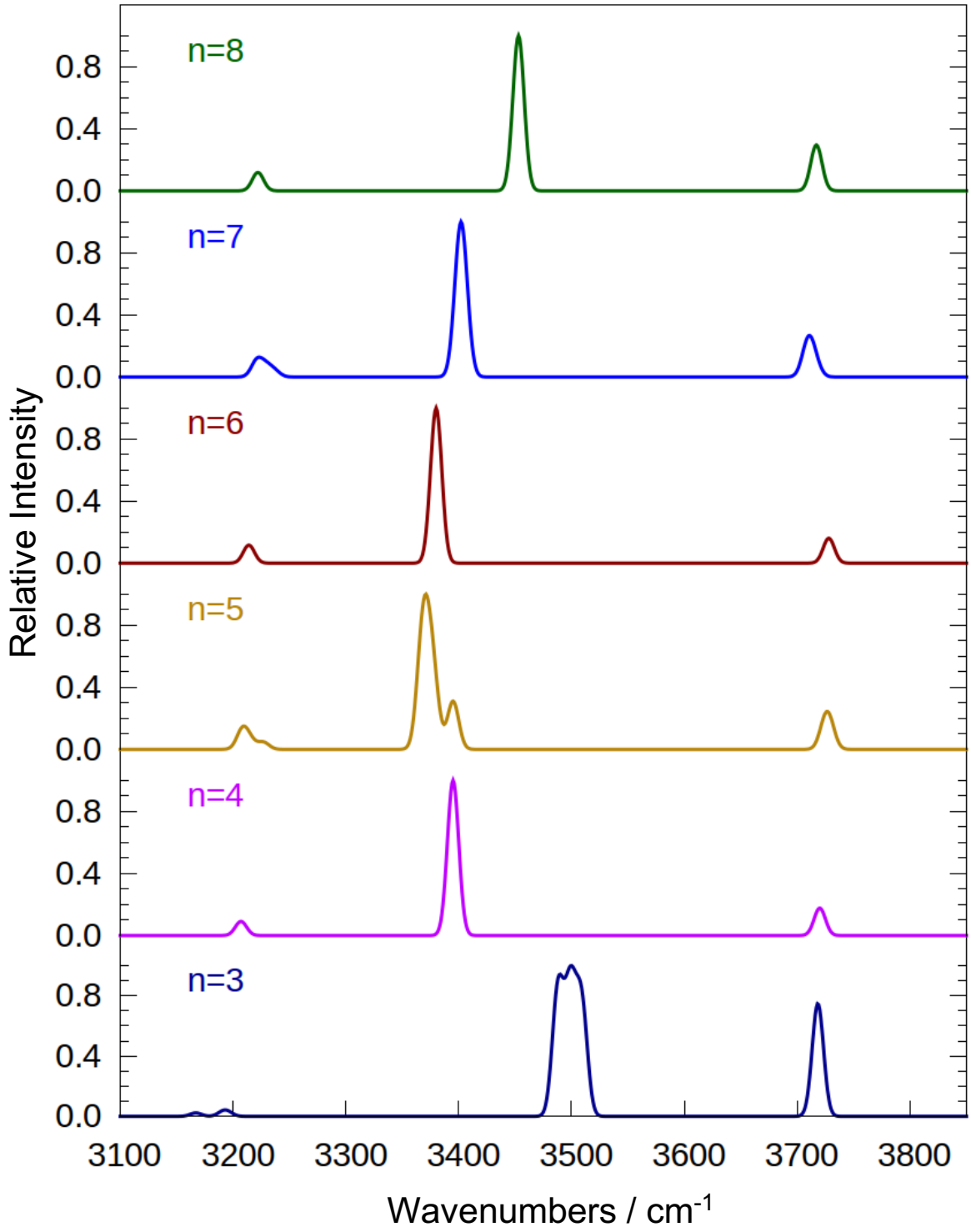

Figure 16: IR spectra of cyclic clusters (n = 3-8) obtained from anharmonic approximations. The vibrational bands on the IR spectra have not been scaled due to their anharmonic origin.

3.2. Methanol-Water Cluster, $MeOH(H_2O)_n$

3.2.1. Optimised Structures

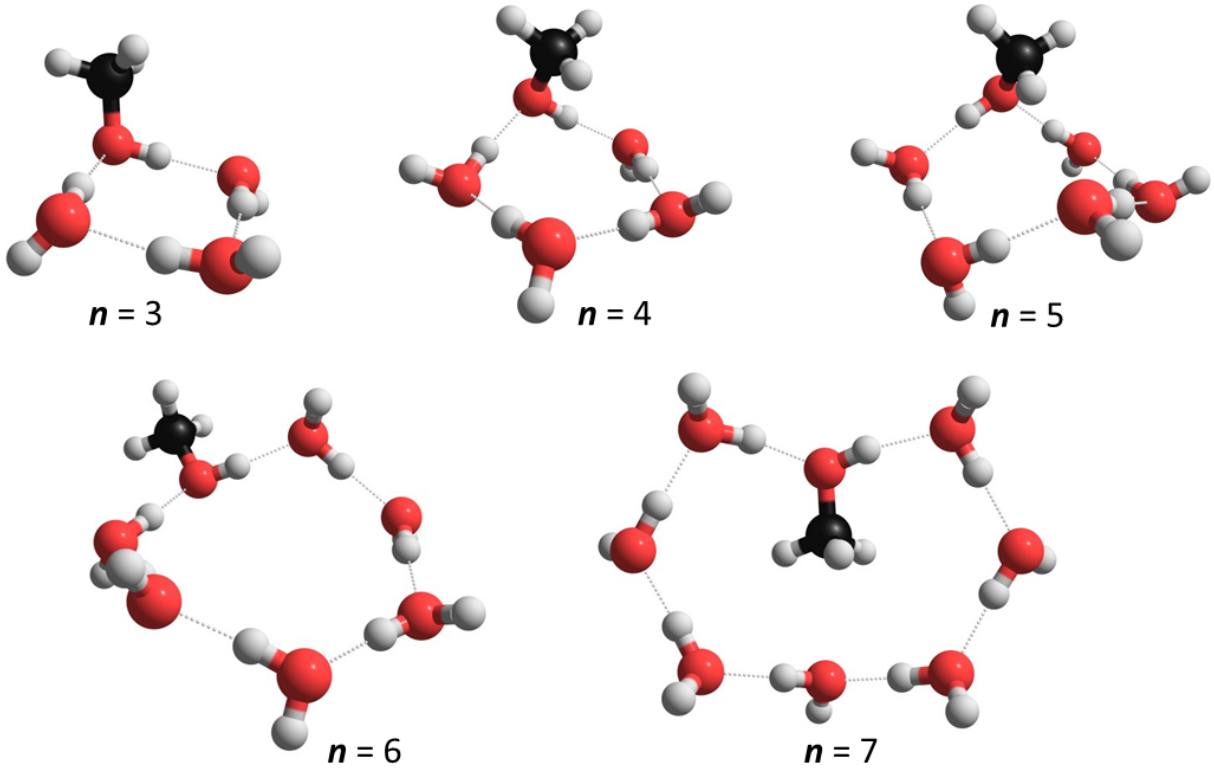

Figure 17: The structures of the cyclic methanol-water clusters optimised at the MP2/aug-cc-pVDZ level. ***n*** represents the number of water molecules within the $MeOH(H_2O)_n$ cluster.

The optimised structures of the methanol-water clusters are presented in **Figure 17**. Theory showed that a methanol molecule is able to fuse into a pre-existing cyclic water clusters. The interaction of the methanol with water monomers is facilitated by the hydroxyl group forming hydrogen bonds with H-atoms and O-atoms from water monomers; this mimics a 2-coordinated water molecule of the donor-acceptor type. From trimer to hexamer cluster sizes the methyl (Me) group of the alcohol molecule avoids being in the centre of the ring where there is maximum interaction with water molecules. In this conformation the hydrophobic group avoids or minimises contact with water.

However, at n = 7 the methyl group was found to be stable in the centre of the ring pointing towards the other water monomer, with then retention of the cyclic structure. This suggested that the $MeOH(H_2O)_7$ (mixed octamer) may be the smallest cluster size that is large enough accommodate polar within the ring. Due to the absence of other methanol molecules hydrophobic hydration cannot occur.[67] The methanol may have flipped the methyl group into the centre of the ring in an attempt minimise strain on the H-bonds. It is believed that not doing so may have led to the formation of larger cyclic cluster leading to an unfavourable increase in the strain energy.

Figure 18 shows the predicted atomic charges which the nature of the electron density distribution around the cyclic cluster. The O-atom in methanol molecule possessed the most negative atomic charge value. This meant that it is has a higher electron density than the O-atoms found in other water molecules in the ring. This electron density stems from the methyl group via inductive electron-donation. As a result of the higher electron density in the hydroxyl oxygen, the H-bond involving the methanol as an acceptor is stronger than the H-bonds from water donors, this is evident from its relatively shorter H-bond length (1.687 Å cf. ~1.738 Å).[26] The formation of this strong H-bond could be a driving force for the insertion of the methanol molecule into cyclic water cluster.

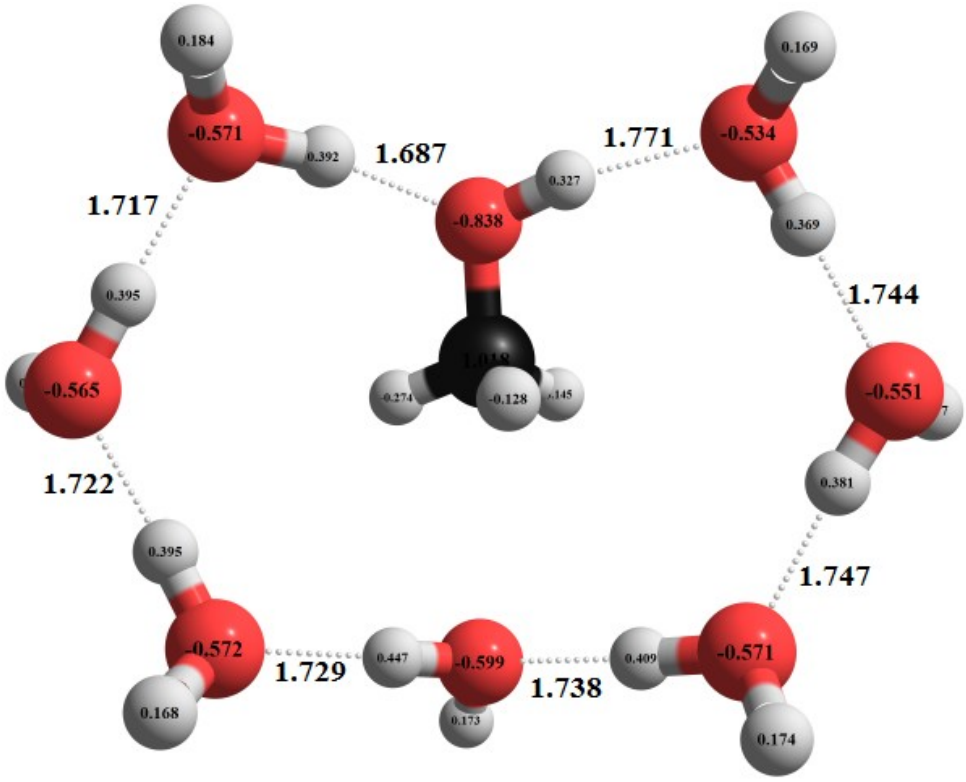

Figure 18: The optimised methanol-heptamer water, $MeOH(H_2O)_7$, cluster is presented with the atomic charges and the hydrogen bond lengths.

3.2.2. IR Spectral Features

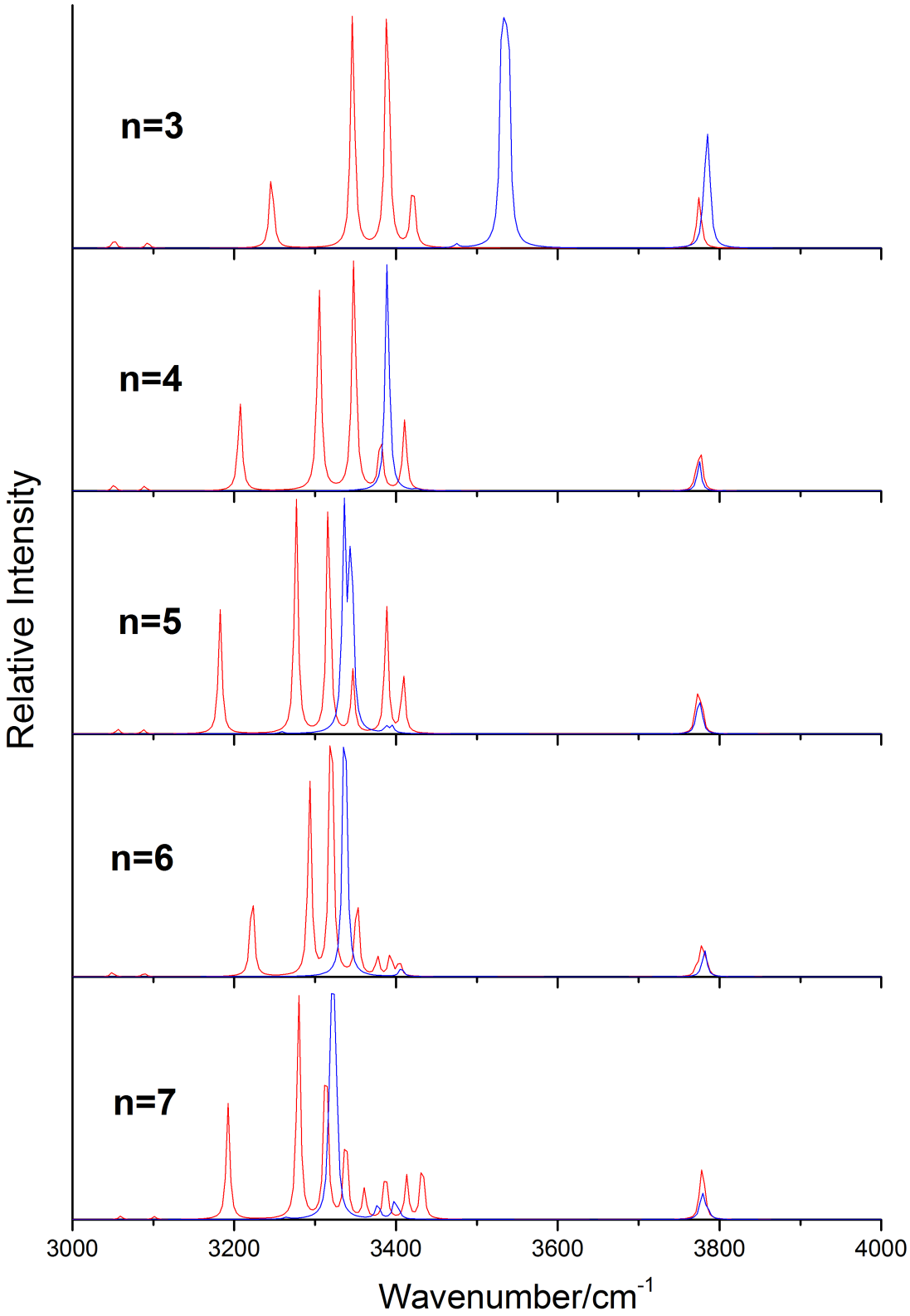

Figure 19: The simulated IR spectra of $MeOH(H_2O)_n$ (red) and $(H_2O)_n$ (blue) clusters are presented in the order of increasing cluster sizes, from **n** = 3 to 7. The vibrational wavenumber has been adjusted using a global scaling factor of 0.972.

The harmonic frequencies and intensities were approximated for the methanol-water clusters and water cluster from the previous section. The simulated IR spectra of pure and mixed water clusters are presented in **Figure 19**. The predicted wavenumbers were adjusted using a global scaling factor of 0.972 which was the coefficient used to scale the most intense band (bonded-OH) for the water clusters. The free-OH bands across all cluster-sizes was fixed at ca. 3790 cm^{-1}. The predicted free-OH stretches arising from the rings in the methanol-water clusters were consistent with those arising from pure water clusters and their band intensities were comparable with each other.

The bonded-OH stretches spanned across from 3180 to 3450 cm^{-1}. The main noticeable difference between the spectra of pure water clusters and those containing the methanol monomer was the splitting of the bonded-OH band into multiple parts. The complexity of the splitting increased with the cluster size and the splitting did not show any apparent patterns. The split bonded-OH bands corresponded to stretches that were out of sync with each other. The splitting of the band may be the cause of the asymmetry introduced by the methanol causing stretches to vibrate at different wavenumbers. However, the splitting was characteristic for every cluster size which means that the presence of different methanol-water clusters can be identified with ease.

For a given cluster with the same of water molecules (n) the bonded-OH band arising from the methanol-water clusters seemed to be at lower wavenumbers compared with the pure water clusters (shown in **Figure 19**). This redshift be explained by the growth of the ring following the addition of a methanol monomer to a pre-existing ring. As consequence of this growth the H-bonds become more strained which reflects in the shift to lower vibrational wavenumbers as the ring size increases.[4] Unfortunately, due to the complexity of this band the redshift could not be quantified.

In the methanol-water cluster spectra two weak bands were observed at 3049 and 3088 cm^{-1}. These peaks correspond to the *anti-symmetric* C-H stretches. As there are many OH bonds present they are bound to produce higher intense peaks. At lower wavenumbers just outside the 3000-4000 cm^{-1} region the *symmetric* C-H stretches were observed at ca. 2967 cm^{-1}. Both C-H were cluster-size independent and relatively weaker compared to the OH stretches. The low intensities of the bands can be explained by the large difference in the number of C-H and O-H bonds present in the cluster.

3.2.3. Proposal for Future Investigations

The mechanism by which the cyclic-$MeOH(H_2O)_n$ clusters would form within helium droplets is currently unknown. One can speculate that this may take place in the following order: (1) The growth of cyclic water clusters via the ring insertion mechanism as proposed by Miller *et al.*[15] (2) The insertion of a single methanol molecule into the pre-existing ring. Whether the insertion of the

methanol can take place via quantum mechanical tunnelling through the associated energy barrier remains to be uncertain and requires further theoretical investigation. Methanol insertion via tunnelling effects may be inhibited because it would involve the motion of heavier atoms compared to water.[15] However, it may be possible that the zero point energy of existing cyclic cluster and some residual kinetic energy that is not removed by the evaporation of helium atoms from the surface of the droplet are sufficient enough for the insertion to take place.[16] One of the important requirements to confirm this hypothesis is the experimental observation of these cyclic clusters.

In the future, the simulated vibrational spectrum reported in this study can be used in parallel with experimental infrared data to confirm the formation of these clusters inside HeNds. Multiple material can be introduced into HeNds via *sequential pickup* method similar to that employed by Ellis *et al.* to form $NaCl(H_2O)_n$.[68] It would require an additional pickup cell further downstream to the existing water pickup cell in the current setup to accommodate the gaseous methanol molecules. As He beam pass through the first pickup cell they capture water molecules and subsequently form water clusters within the droplet. Afterwards, the droplet takes up methanol molecules as it travels through the second pickup cell. The pressure of the second pickup is required to be relatively lower than that of the first in order to form water-rich clusters.

Despite the pressure control, sequential insertion will lead to the formation of a number of different sized methanol-water aggregates and thus a size-selective is necessary for recording the IR absorption spectra. Shi *et al.* found that ionisation of mixed water-methanol leads to the protonation of the cluster, leading to the formation of $(MeOH)(H_2O)_mH^+$ ion, where $m = n - 1$.[36] Thus, by recording the depletion spectra of the $(MeOH)(H_2O)_mH^+$ ion it will be possible to obverse important vibrational contribution arising from the neutral cluster, $(MeOH)(H_2O)_m$. The structural assignment of a specific cyclic $MeOH(H_2O)_n$ cluster is possible by the presence of the free-OH stretches and the split bonded-OH stretches which is unique for each cluster size (n). The complex nature of the bonded-OH band makes it difficult to focus on OH stretch vibrations arising from only methanol or water molecules. Huisken *et al.* demonstrated that it is possible to focus on the OH absorption band of methanol by using deuterated water, D_2O.[37] Vibrational frequency of oxygen-deuterium stretches would absorb in the same spectral region and this prevents the perturbation of the methanol OH stretches by water molecules.

3.3. Hydrogen-Water Cluster, $H_2(H_2O)_n$

3.3.1. Structural Analysis of Optimised Cluster

The geometry optimisation was carried out on a hexamer ring, which contained a dihydrogen molecule in the centre of the cluster. The water hexamer model used in this optimisation was pre-optimised, which made it possible to observe the changes in its structure after loading the H_2. **Figure 20** presents the structures of the $H_2(H_2O)_6$ cluster before and after the optimisation. Prior to the optimisation the dihydrogen molecule was located in the centre of the cyclic water cluster. However, the optimised structure revealed that the hydrogen prefers to maintain a distance from the ring rather remain in the centre. Pascal *et al.* suggested that the quadrupole (H_2) – dipole (H_2O) interaction stabilises the H_2 – ice structure, with the Van der Waals' (VdW) forces always repulsive to counter-act the favourable electrostatic forces.[42] These repulsion forces may be the reason why the hydrogen keeps a separation (~ 2 Å) keeps from the ring.

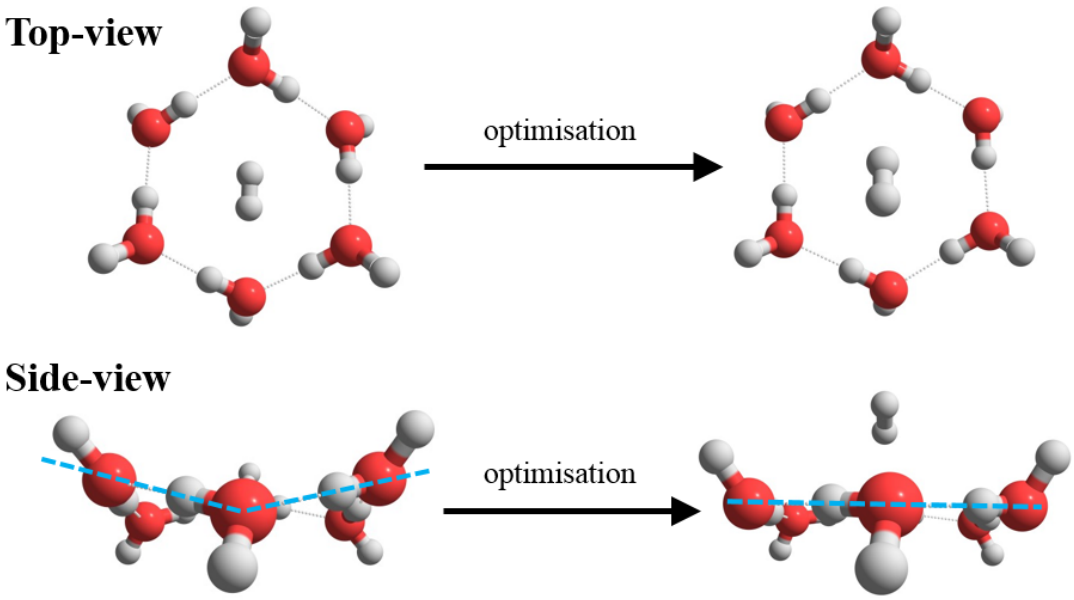

Figure 20: Top-view and side-view of the $H_2(H_2O)_6$ cluster model before and after geometry optimisation. The dashed line (in the side-view representation) helps to see the change in the water cluster geometry.

A remarkable observation was the change in the cyclic hexamer geometry following the optimisation. The ring, which was of a quasi-planar nature, seemed to have turned 'more' planar. This can be seen in the side-view illustration of the cluster in **Figure 20**. The cyclic hexamer has a quasi-planar structure similar to the *chair* conformation observed for cyclohexane. The chair conformation minimises the strain energy that exists within the ring.[69] Therefore, the transformation of the quasi-planar ring to a relatively more 'planar' suggested that this must be facilitated by stabilisation

provided by the dihydrogen molecule. The complete influence of this small molecular change on the macroscopic property of ice is unknown, but this structural change could be a contributing factor for the efficient hydrogen storage.

3.3.2. Electron Density

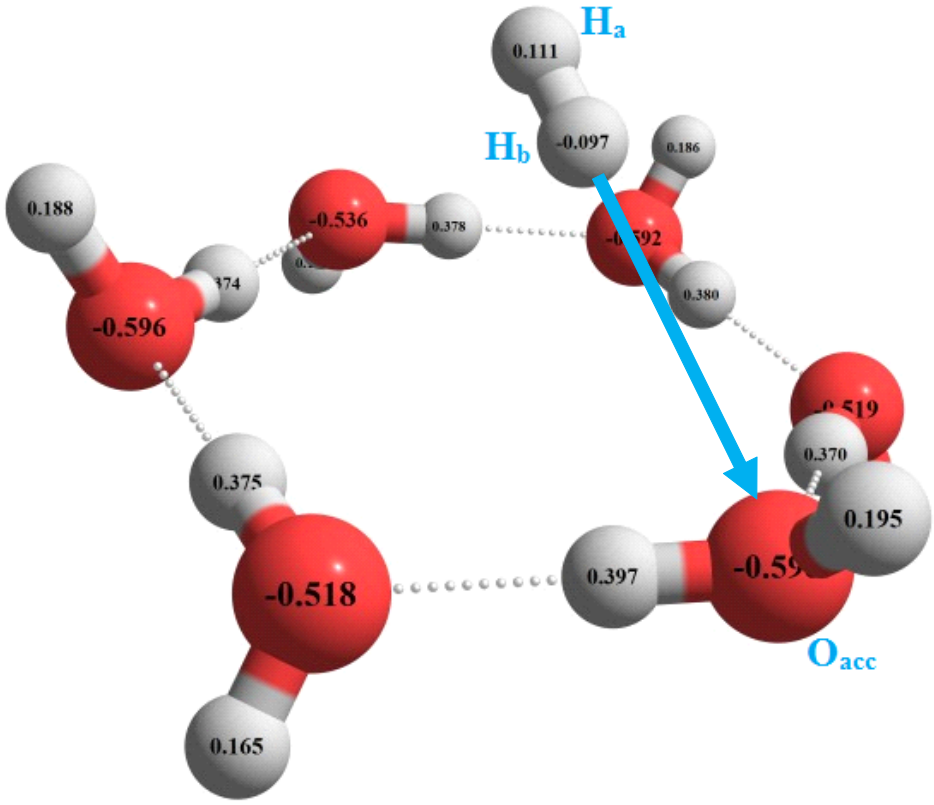

Figure 21: A perspective view of the optimised $H_2(H_2O)_6$ cluster with predicted atomic charges. H_a-atom donates electron-density to H_b-atom, which in turn enables the long-range VdW attractive interaction with O_{acc}. The blue arrow indicates this small donation of electron density from H_b and O_{acc}.

As seen in **Figure 20**, the hydrogen molecule was is not directly bound to any water molecules. The reason they cannot form H-bonds lies due to the lack of polarity in H_2. Nevertheless, a closer look at the atomic charges of the individual atoms in the clusters help to understand the VdW interaction between the $(H_2O)_6$ and H_2.[70] The fact that one H-atom (H_a) in H_2 possesses a positive atomic charge while the other H-atom (H_b) has negative suggests that the diatomic molecule is polarised (see **Figure 21**). The polarisation is believed to be influenced by the electronegative oxygen atom (O_{acc}) found on the closest water monomer to the H_2. This is evident from H_b-atom having partial atomic charge of -0.097 and the H_2 diatomic pointing towards O_{acc}, which is predicted to be the most electronegative atom with an atomic charge of -0.598. The H_2 molecule adopts a tilted position which may be to maximise the VdW interaction with O_{acc}. This attraction is not felt by H_b atom possibly because the adjacent oxygen atom is not electronegative enough.

The finding helped capture a better picture of the hydrogen-water interaction. H_b-atom receives a small amount of electron density from H_a-atom due to polarisation of the diatomic molecule when in close proximity to the cyclic hexamer. Some electron density is being donated by H_b-atom to the O_{acc}-atom, which *accepts* it. The sharing of the electron density by H_b and O_{acc} gives rise to the long range VdW interactions. It may also be the case that oxygen atoms on other water molecules involved in the interaction, but there is no direct evidence to support this hypothesis.

3.3.3. Simulated IR spectra

As mentioned previously, the vibrational frequencies of the bonded-OH stretches is sensitive to the changes in the cluster geometry which in turn triggers a change in the H-bonds.[71] Therefore, any structural changes to the cyclic hexamer resulted from loading of hydrogen was expected to induce a shift in the bonded-OH band position. **Figure 22** presents the simulated infrared spectrum for the optimised $H_2(H_2O)_6$ and $(H_2O)_6$ clusters. Comparison of the spectrum predicts that the free-OH band redshifts by 5 cm^{-1} following the addition of a hydrogen molecule. This small shift may have arisen from the Van der Waal's interaction (attraction/repulsive) of the H_2 with the free-OH stretches, which may slightly restrict the vibration leading to a reduction in its vibrational frequency.

The bonded-OH stretches of the cyclic hexamer in the hydrogen-water cluster was located at 3322 cm^{-1}, redshifted by ca. 14 cm^{-1} from the bonded-OH band observed in the pure water cluster. Redshifts in bonded-OH stretches was also observed in cyclic water clusters with increasing cluster

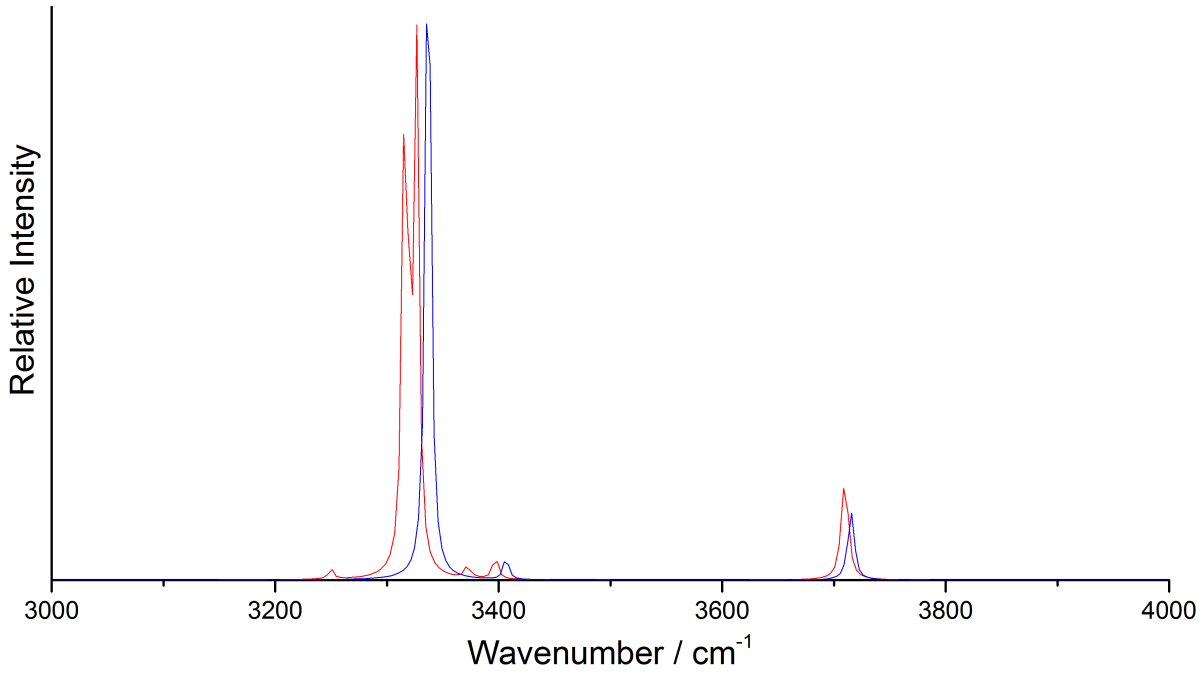

Figure 22: Simulated infrared spectrum of the $H_2(H_2O)_6$ (red) and $(H_2O)_6$ (blue) cluster. The bonded-OH bands were scaled by 0.972 and the free-OH bands by 0.955.

size, from trimer up to the heptamer. Similarly, the redshift in the hydrogen-water cluster could be understood in terms of strain on the H-bonds. The redshift suggests that the loading of H_2 onto the cyclic hexamer results in a structural deformation of the ring which relieves the strain that is put on the H-bonds. This relief may be the driving force behind the stable storage of hydrogen within hexagonal ice because chemical systems prefer adapt conformation that lowers its internal energy, minimising any strain energy. The average H-bond length has reduced from ~1.745 to ~1.373 Å, indicating strengthening of the H-bonds after H_2 loading. Another interesting spectroscopic feature was the noticeable splitting of the bonded-OH band into two vibrational transitions separated by approx. 10 cm^{-1}. This separation was present in the pure water cluster, but it was relatively smaller (2 cm^{-1}). This large splitting could be attributed to the asymmetry introduced by the hydrogen molecule, causing the bonded-OH vibrational stretches to take place at two different frequencies.

The band corresponding to the symmetric H-H stretching of the diatomic hydrogen molecule was located at 4325 cm^{-1} (scaled by 0.972). The intensity of this band was very low compared to the OH stretches which can be accounted for by the large difference in the number of O-H and H-H bonds present in the hydrogen-water cluster. Harmonic frequency calculation of a free dihydrogen molecule carried out at the MP2/aug-cc-pVDZ level predicted this band at 4338 cm^{-1}. The 13 cm^{-1} red shift suggests weakening of the bonds which may be the result of the Van der Waal's interaction with the water cluster.

3.3.4. Proposal for Future Investigations

Following the theoretical analysis of the hydrogen-water cluster, the next logical step is to confirm the existence of this cluster via experimental methods. The predicted vibrational wavenumbers reported in this theoretical investigation can also be used in conjunction with experiments to confirm the formation of the hydrogen-hexamer cluster inside HeNds.

This carried out by forming the mixed cluster inside HeNds using sequential insertion and studying using a similar setup described in the experimental. Assuming the ionisation of hydrogen-water clusters occur via the formation of protonated clusters similar to pure water cluster, the IR absorption spectra of $H_2(H_2O)_6$ could be obtained using RIDIRS of mass channel 111 which corresponds to $H_2(H_2O)_6H^+$ ion. The formation of the $H_2(H_2O)_6$ cluster within NeNds can be confirmed by the presence of the split bonded-OH band at ca. 3322 cm^{-1} and free-OH at ca. 3710 cm^{-1} in the size-selected IR spectrum. The weak H_2 stretch at 4325 cm^{-1} may not be clearly visible in the experiment due to the noise/fluctuations in the signal. In addition to these bands, the band corresponding to the OH bend-overtone is expected at approximately 3229 cm^{-1}.[23]

Further *ab initio* theoretical investigation would shine a light on the nature of the stabilisation that hydrogen provides for the ring. For example, binding energies of water cluster help determine the hydrogen bond energy and as the cyclic hexamer with the hydrogen is believed to relieve strain on the hydrogen bonds, it is expected that hydrogen bond energy of the ring must be lower compared to the ring on their own.[72,73] Thus, by predicting the binding energies (using counterpoise corrections) the stabilisation provided by hydrogen loading could be quantified. These insights could provide information to improve the current hydrogen storage mediums and therefore, hydrogen-water cluster will be an interesting area to explore in the future studies. The present part of the study ignites many questions such as whether the stabilisation is limited to only one hydrogen molecule and whether larger water clusters ($n > 7$) are able to provide similar stabilisation to accommodate hydrogen within their H-bond network.

CHAPTER 4 CONCLUSION

4.1. Water Clusters, $(H_2O)_n$

Water clusters were successfully formed inside HeNds as evident from the presence of protonated water clusters, $(H_2O)_mH^+$, in the mass spectrum of doped HeNds. RIDIRS of the $H^+(H_2O)_6$ ion allowed to measure size-selective vibrational stretches arising neutral heptamer cluster, $(H_2O)_7$. Different structural conformers (prism, cage, bicyclic and cyclic) of the heptamer were optimised compared to the recorded spectrum. The IR spectrum of the heptamer was consistent with the theoretical predictions corresponding to the cyclic conformer. This finding was supported by the good agreement between experimental and scaled-harmonic wavenumbers.

The shifts in the bonded-OH bands of the cyclic clusters ($3 \leq n \leq 8$) was an indicator of strain on the H-bonds. Experiment and theory indicated that the bonded-OH band arising from the cyclic heptamer is the most redshifted one. This suggested that heptamer may be the ring with the lowest structural strain and possesses minimum strain energy compared to other cyclic water clusters ($n < 8$). For the cyclic heptamer, the anharmonic approximation predicted the bonded-OH at wavenumbers 60 cm^{-1} than those obtained from the experiment and harmonic calculations. The large discrepancy may be the result of comparing wavenumbers that stem from different cyclic conformers of the heptamer and therefore these results were of little importance. Nevertheless, the predicted bend overtone band position was in good agreement with the experiment. The theory indicated that the bonded-OH band in the heptamer IR spectrum was consisted of two vibrational transitions. Of the two transitions the lower wavenumber transition (at 3415 cm^{-1}) had a transition dipole moment along the permanent dipole moment, which was agreed with the experimental Stark measurements reported by Miller *et al*.[16]

The observation of cyclic heptamer was made despite a number of previous experiments and theoretical studies confirming that the heptamer has a preference for a 3D prism structure as the minimum energy conformation. This means that Miller and co-worker's proposed sequential *ring insertion* mechanism is also valid for the heptamer.[16] The hypothesis is that the cyclic heptamer is formed through the following order: **(1)** the formation of minimum-energy small cyclic clusters (n = 3-5) **(2)** subsequent addition of two water monomers via quantum tunnelling through the associated energy barriers. The newly formed ring could not have relaxed to the low-energy prism structure as the rearrangement of the hydrogen bond network would require the breaking and forming of multiple hydrogen bonds; this can neither be facilitated by overcoming the associated energy barrier nor

quantum tunnelling through the barrier. It is believed that the addition of heptamer to the existing family of cyclic water cluster will help study cooperativity effects in future work.

The technique employed in the present study was straightforward and proved to be a promising tool to obtain details about the H-bond network of clusters. However, the major drawback of this is approach is that prerequisite knowledge of the approximate cluster structure is required for the spectral assignment. Furthermore, the size of the clusters that can be analysed using this technique is limited by computational cost of *ab initio* calculations. It would be computationally expensive and inefficient to run an *ab initio* optimisation calculation on every possible cluster for a given cluster size. In addition to this, identifying the necessary local minima on the complex PES of larger water clusters ($n > 10$) is anticipated to be greatly difficult. To tackle this problem this technique can benefit from Molecular Mechanical calculations, which are much faster and could aid in narrowing down the probable cluster geometries to be sampled using *ab initio* method.

4.2. Methanol-Water Cluster, $MeOH(H_2O)_n$

Methanol-water mixtures has been of subject to extensive studies. In this theoretical work the local minima of cyclic-$MeOH(H_2O)_n$ clusters (where $n = 3 - 7$) were identified at the MP2/aug-cc-pVDZ level. The finding showed that the methanol molecule is hydrogen-bonded as a proton donor and single acceptor to two water molecules. The predicted atomic charges revealed elevated electron density at the hydroxyl oxygen due to electron-density donation from the methyl group. The mixed octamer cluster, $MeOH(H_2O)_7$, was found to be the smallest ring that is capable to accommodate the methyl group at the centre of the ring.

Following the methanol insertion, the bonded-OH stretches of the cyclic clusters were found to have redshifted as the result of the increased strain on the H-bonds. Theory suggested that the bonded-OH bands split into multiple transitions due to loss of symmetry caused by the presence of the methanol monomer. However, these split bands are unique and can be used to identify ring size which they arise from. The free-OH stretches at approx. 3790 cm^{-1} remained unaffected by methanol insertion. Very weak, cluster size independent bands corresponding to anti-symmetrical and symmetrical C-H stretches were identified at 3049 – 3088 cm^{-1} and 2967 cm^{-1}, respectively.

It was assumed that the formation of these clusters is possible by insertion of methanol into a pre-existing cyclic water cluster. Although this insertion may not be facilitated by quantum mechanical tunnelling due to the motion of heavy atoms, the ZPE of the clusters could be sufficient enough to assist the motion. It is anticipated that the reported spectral features of these cyclic clusters will be useful to confirm the formation of these clusters inside helium droplets when used in conjunction with experimental infrared spectra. Suggestions for studying methanol-water clusters for

future experimental work has been proposed in the present study. It is believed that these cyclic clusters and similar cyclic mixed clusters will serve as a better prototype in upcoming work to explore the intermolecular interaction.

4.3. Hydrogen-Water Cluster, $H_2(H_2O)_n$

The final part of the investigation examined the hydrogen stabilisation effect on the cyclic hexamer, which leads to efficient hydrogen gas storage in ice, particularly hexagonal ice. This was achieved by analysing structural parameters and comparing predicted vibrational spectrum of that of the $H_2(H_2O)_6$ cluster to that of the cyclic hexamer. The interaction was understood from the structural change that the cyclic hexamer underwent after loading a dihydrogen molecule.

The optimised structure indicated that a dihydrogen can be stable in a cyclic framework of water molecules. Van der Waal's forces which attracts the H_2 to cyclic hexamer cluster is also responsible for repulsion forces acting between two components, resulting in a separation. The H_2 becomes mildly polarised near the presence of the cyclic hexamer, resulting on of the H-atom to donate electron density over to an O-atom in the cluster. This observation was derived from the predicted atomic charges and helped to explain the tilted orientation of the diatomic H_2 in the optimised structure. The redshift of the bonded-OH band suggested that the loading of one H_2 molecule onto a cyclic hexamer leads to the reduction of the structural strain.

For the *ab initio* study, the cyclic hexamer was a suitable substitute to represent the hexagonal ice because the geometry optimisation of hexagonal ice lattice would have been computationally expensive and hence difficult. The spectral features of OH-stretches have been reported $H_2(H_2O)_6$ cluster has been discussed for future experimental work. In addition to this, suggestions for future theoretical exploration of hydrogen-water clusters have also been proposed. It is believed that this finding will turn more attention towards ice-based hydrogen storage and contribute towards making hydrogen fuel a viable energy in the near future.

CHAPTER 5 REFERENCES

1. R. Ludwig, *Angewandelte Chem.*, 2001, **40**, 1801–1827.
2. S. Harrington, R. Zhang, P. H. Poole, F. Sciortino and H. E. Stanley, *Phys. Rev. Lett.*, 1997, **78**, 2409–2412.
3. K. Liu, J. D. Cruzan and R. J. Saykally, *Science*, 1996, **271**, 929–933.
4. F. N. Keutsch and R. J. Saykally, *Proc. Natl. Acad. Sci.*, 2001, **98**, 10533–10540.
5. R. Bukowski, K. Szalewicz, G. C. Groenenboom and A. van der Avoird, *Science*, 2007, **315**, 1249–1252.
6. H. C. Hailes, *Org. Process Res. Dev.*, 2007, **11**, 114–120.
7. A. Luzar and D. Chandler, *Phys. Rev. Lett.*, 1996, **76**, 928–931.
8. J. K. Gregory and D. C. Clary, *J. Phys. Chem.*, 1996, **100**, 18014–18022.
9. R. N. Pribble and T. S. Zwier, *Science*, **265**, 75–79.
10. C. Perez, M. T. Muckle, D. P. Zaleski, N. A. Seifert, B. Temelso, G. C. Shields, Z. Kisiel and B. H. Pate, *Science*, 2012, **336**, 897–901.
11. U. Góra, R. Podeszwa, W. Cencek and K. Szalewicz, *J. Chem. Phys.*, 2011, **135**, 224102.
12. Y. Wang, B. C. Shepler, B. J. Braams and J. M. Bowman, *J. Chem. Phys.*, 2009, **131**, 054511.
13. Y. Wang, X. Huang, B. C. Shepler, B. J. Braams and J. M. Bowman, *J. Chem. Phys.*, 2011, **134**, 094509.
14. F. C. Hagemeister, C. J. Gruenloh and T. S. Zwier, *J. Phys. Chem. A*, 1998, **102**, 82–94.
15. K. Nauta and R. E. Miller, *Science*, 2000, **287**, 293–295.
16. R. E. Miller, B. E. Applegate, M. A. Miller, C. J. Burnham and S. S. Xantheas, *J. Chem. Phys.*, 2002, **117**, 1109–1122.
17. T. S. Zwier, *Annu. Rev. Phys. Chem.*, 1996, **47**, 205–241.
18. M. B. Day, K. N. Kirschner and G. C. Shields, *J. Phys. Chem. A*, 2005, **109**, 6773–6778.
19. B. Temelso, K. A. Archer and G. C. Shields, *J. Phys. Chem. A*, 2011, **115**, 12034–12046.
20. D. M. Bates and G. S. Tschumper, *J. Phys. Chem. A*, 2009, **113**, 3555–3559.
21. K. Kim, K. D. Jordan and T. S. Zwier, *J. Am. Chem. Soc.*, 1994, **116**, 11568–11569.
22. J. Y. Lee, *Chem. Phys.*, 2004, **299**, 123–129.
23. Y. Wang and J. M. Bowman, *J. Phys. Chem. Lett.*, 2013, **4**, 1104–1108.
24. K. Ohno, M. Okimura, N. Akai and Y. Katsumoto, *Phys. Chem. Chem. Phys.*, 2005, **7**, 3005.
25. J. M. Guevara-Vela, R. Chávez-Calvillo, M. García-Revilla, J. Hernández-Trujillo, O. Christiansen, E. Francisco, Á. Martín Pendás and T. Rocha-Rinza, *Chem. - Eur. J.*, 2013, **19**, 14304–14315.
26. A. Mandal, M. Prakash, R. M. Kumar, R. Parthasarathi and V. Subramanian, *J. Phys. Chem. A*, 2010, **114**, 2250–2258.
27. R. M. Shields, B. Temelso, K. A. Archer, T. E. Morrell and G. C. Shields, *J. Phys. Chem. A*, 2010, **114**, 11725–11737.

28. C. Pérez, S. Lobsiger, N. A. Seifert, D. P. Zaleski, B. Temelso, G. C. Shields, Z. Kisiel and B. H. Pate, *Chem. Phys. Lett.*, 2013, **571**, 1–15.
29. N. Acelas, G. Hincapié, D. Guerra, J. David and A. Restrepo, *J. Chem. Phys.*, 2013, **139**, 044310.
30. J. Kim, D. Majumdar, H. M. Lee and K. S. Kim, *J. Chem. Phys.*, 1999, **110**, 9128–9134.
31. J. Gelman Constantin, A. Rodriguez Fris, G. Appignanesi, M. Carignano, I. Szleifer and H. Corti, *Eur. Phys. J. E*, 2011, **34**, 126.
32. L. Dougan, S. P. Bates, R. Hargreaves, J. P. Fox, J. Crain, J. L. Finney, V. Réat and A. K. Soper, *J. Chem. Phys.*, 2004, **121**, 6456–6462.
33. R. A. Provencal, J. B. Paul, K. Roth, C. Chapo, R. N. Casaes, R. J. Saykally, G. S. Tschumper and H. F. Schaefer, *J. Chem. Phys.*, 1999, **110**, 4258–4267.
34. R. N. Pribble, F. C. Hagemeister and T. S. Zwier, *J. Chem. Phys.*, 1997, **106**, 2145.
35. A. Wakisaka, H. Abdoul-Carime, Y. Yamamoto and Y. Kiyozumi, *J. Chem. Soc. Faraday Trans.*, 1998, **94**, 369–374.
36. Z. Shi, S. Wei, J. V. Ford and A. W. Castleman, *Chem. Phys. Lett.*, 1992, **200**, 142–146.
37. F. Huisken, S. Mohammad-Pooran and O. Werhahn, *Chem. Phys.*, 1998, **239**, 11–22.
38. T. Sato, A. Chiba and R. Nozaki, *J. Chem. Phys.*, 2000, **112**, 2924–2932.
39. G. Cipriani, V. Di Dio, F. Genduso, D. La Cascia, R. Liga, R. Miceli and G. Ricco Galluzzo, *Int. J. Hydrog. Energy*, 2014, **39**, 8482–8494.
40. M. Lancaster, *Green chemistry: an introductory text*, Royal Society of Chemistry, Cambridge, 2nd ed., 2010, p. 217.
41. H. Furukawa and O. M. Yaghi, *J. Am. Chem. Soc.*, 2009, **131**, 8875–8883.
42. T. A. Pascal, C. Boxe and W. A. Goddard, *J. Phys. Chem. Lett.*, 2011, **2**, 1417–1420.
43. A. H. Nguyen and V. Molinero, *J. Phys. Chem. B*, 2015, **119**, 9369–9376.
44. G. P. Moss, P. A. S. Smith and D. Tavernier, *Pure Appl. Chem.*, 1995, **67**, 1328.
45. W. L. Mao, *Science*, 2002, **297**, 2247–2249.
46. J. F. Allen and A. D. Misener, *Nature*, 1938, **141**, 75.
47. A. De Troyer, A. Van Itterbeek and G. . Van Den Berg, *Physica*, 1951, **17**, 50–62.
48. L. Landau, *Phys. Rev.*, 1941, **60**, 356–358.
49. M. Hartmann, R. E. Miller, J. P. Toennies and A. F. Vilesov, *Science*, 1996, **272**, 1631–1634.
50. S. Yang and A. M. Ellis, *Chem Soc Rev*, 2013, **42**, 472–484.
51. J. P. Toennies and A. F. Vilesov, *Angew. Chem. Int. Ed.*, 2004, **43**, 2622–2648.
52. L. F. Gomez, E. Loginov, R. Sliter and A. F. Vilesov, *J. Chem. Phys.*, 2011, **135**, 154201.
53. N. Halberstadt and K. C. Janda, *Chem. Phys. Lett.*, 1998, **282**, 409–412.
54. A. M. Ellis and C. A. Mayhew, *Proton transfer reaction mass spectrometry: principles and applications*, New York, GB, 2014, p. 81.
55. F. Stienkemeier and K. K. Lehmann, *J. Phys. B At. Mol. Opt. Phys.*, 2006, **39**, R127–R166.
56. R. N. Pribble, A. W. Garrett, K. Haber and T. S. Zwier, *J. Chem. Phys.*, 1995, **103**, 531–544.

57. U. Buck and F. Huisken, *Chem. Rev.*, 2000, **100**, 3863–3890.

58. F. Jensen, *Introduction to computational chemistry*, John Wiley & Sons, Chichester, England ; Hoboken, NJ, 2nd ed., 2007, p. 22 & 159–162.

59. B. Santra, A. Michaelides and M. Scheffler, *J. Chem. Phys.*, 2007, **127**, 184104.

60. T. H. Dunning, *J. Chem. Phys.*, 1989, **90**, 1007–1023.

61. R. A. Kendall, T. H. Dunning and R. J. Harrison, *J. Chem. Phys.*, 1992, **96**, 6796–6806.

62. A. Vila Verde, P. G. Bolhuis and R. K. Campen, *J. Phys. Chem. B*, 2012, **116**, 9467–9481.

63. M. N. Slipchenko, S. Kuma, T. Momose and A. F. Vilesov, *Rev. Sci. Instrum.*, 2002, **73**, 3600–3605.

64. K. Nauta and R. E. Miller, *Phys. Rev. Lett.*, 1999, **82**, 4480–4483.

65. J. Brudermann, M. Melzer, U. Buck, J. K. Kazimirski, J. Sadlej and V. Bush, *J. Chem. Phys.*, 1999, **110**, 10649–10652.

66. O. M. Becker and M. Karplus, *J. Chem. Phys.*, 1997, **106**, 1495–1517.

67. J. Israelachvili and R. Pashley, *Nature*, 1982, **300**, 341–342.

68. J. Tandy, C. Feng, A. Boatwright, G. Sarma, A. M. Sadoon, A. Shirley, N. D. N. Rodrigues, E. M. Cunningham, S. Yang and A. M. Ellis, *J. Chem. Phys.*, 2016, **144**, 121103.

69. J. Clayden, N. Greeves and S. G. Warren, *Organic chemistry*, Oxford University Press, Oxford ; New YorK, 2nd ed., 2012, p. 370–373.

70. A. H. Pakiari and S. Fakhraee, *J. Theor. Comput. Chem.*, 2006, **5**, 621–631.

71. F. N. Keutsch, R. S. Fellers, M. G. Brown, M. R. Viant, P. B. Petersen and R. J. Saykally, *J. Am. Chem. Soc.*, 2001, **123**, 5938–5941.

72. R. D. Bach and O. Dmitrenko, *J. Am. Chem. Soc.*, 2004, **126**, 4444–4452.

73. M. W. Feyereisen, D. Feller and D. A. Dixon, *J. Phys. Chem.*, 1996, **100**, 2993–2997.